Remote Sensing of Environment 280 (2022) 113142

Contents lists available at ScienceDirect

Remote Sensing of Environment

journal homepage: www.elsevier.com/locate/rse

Properties of aerosol and surface derived from OLCI/Sentinel-3A using GRASP approach: Retrieval development and preliminary validation

Cheng Chen [a,*], Oleg Dubovik [b,*], Pavel Litvinov [a], David Fuertes [a], Anton Lopatin [a], Tatyana Lapyonok [b], Christian Matar [a], Yana Karol [a], Juergen Fischer [c], Rene Preusker [c], Andreas Hangler [d], Michael Aspetsberger [d], Lukas Bindreiter [d], Daniel Marth [d], Julien Chimot [e], Bertrand Fougnie [e], Thierry Marbach [e], Bojan Bojkov [e]

[a] GRASP-SAS, Villeneuve d'Ascq, France
[b] Univ. Lille, CNRS, UMR 8518 - LOA - Laboratoire d'Optique Atmosphérique, F-59000 Lille, France
[c] Free University of Berlin, Berlin, Germany
[d] Cloudflight Austria GmbH, High Performance Computing, Linz, Austria
[e] EUMETSAT, Darmstadt, Germany

ARTICLE INFO

Edited by Menghua Wang

Keywords:
OLCI/Sentinel-3A
Satellite remote sensing
Aerosol and surface characterization
GRASP algorithm

ABSTRACT

The Ocean and Land Color Instrument (OLCI) onboard the Copernicus Sentinel-3A satellite is a medium-resolution and multi-spectral push-broom imager acquiring radiance in 21 spectral bands covering from the visible to the far near-infrared. These measurements are primary dedicated to land & ocean color applications, but actually include also reliable information for atmospheric aerosol and surface brightness characterization. In the framework of the EUMETSAT funded study to support the Copernicus Program, we describe the retrieval of aerosol and surface properties from OLCI single-viewing multi-spectral Top-Of-Atmosphere (TOA) radiances based on the Generalized Retrieval of Atmosphere and Surface Properties (GRASP) algorithm. The high potential of the OLCI/GRASP configuration stems from the attempt to retrieve both aerosol load and surface reflectance simultaneously using a globally consistent high-level approach. For example, both over land and ocean surfaces OLCI/GRASP uses 9 spectral channels (albeit with different weights), strictly the same prescribed aerosol models and globally the same a priori constraints (though with some differences for observations over land and ocean). Due to the lack of angular multi-viewing information, the directional properties of underlying surface are strongly constrained in the retrieval: over ocean the Fresnel reflection together with foam/whitecap albedo are exclusively computed using a priori wind speed; over land, the Bidirectional Reflectance Distribution Function (BRDF) is slightly adjusted from a priori values of climatological Ross-Li volumetric and geometric terms. Meanwhile, the isotropic reflectance is retrieved globally under mild spectral smoothness constraints. It should be noticed that OLCI/GRASP configuration employs innovative multi-pixel concept (Dubovik et al., 2011) that enhance retrieval by simultaneously inverting large group of pixels. The concept allows for benefiting from knowledge about natural variability of the retrieved parameters.

The obtained OLCI/GRASP products were validated with the Aerosol Robotic Network (AERONET) and Maritime Aerosol Network (MAN) and intercompared with the Moderate Resolution Imaging Spectroradiometer (MODIS) aerosol and surface products. The overall performance is quite comparable to the community-referenced MODIS. Over ocean the OLCI/GRASP results are encouraging with 67% of the AOD (550 nm) satisfying the Global Climate Observing System (GCOS) requirement using AERONET coastal sites and 74% using MAN deep ocean measurements, and an AOD (550 nm) bias 0.01 with AERONET and nearly zero bias with MAN. Over land, 48% of OLCI/GRASP AOD (550 nm) satisfy the GCOS requirement and a bias within ± 0.01 for total and AOD < 0.2. Key challenges are identified and discussed: adequate screening of cloud contaminations, retrieval of aerosol over bright surfaces and in the regions containing complex mixtures of aerosol.

* Corresponding authors.
E-mail addresses: cheng.chen@grasp-sas.com (C. Chen), oleg.dubovik@univ-lille.fr (O. Dubovik).

https://doi.org/10.1016/j.rse.2022.113142
Received 4 February 2022; Received in revised form 26 May 2022; Accepted 19 June 2022
Available online 9 July 2022

1. Introduction

The remote sensing of atmospheric aerosols from space-borne sensors has been progressing for decades. At present, derived satellite products play a vital role in monitoring and understanding atmospheric aerosol spatial distribution, variability, as well as aerosol dynamic processes. Furthermore, a growing number of space-borne instruments has been deployed in Low Earth Orbit (LEO), Geostationary orbit (GEO) and even in deep space Sun-Earth Lagrange L1 Point that can provide valuable information of atmosphere and its underlaying surface. The fundamental challenge for deriving aerosol information from the Top-Of-Atmosphere (TOA) measured radiance is atmosphere-surface signal decoupling (King et al., 1999; Kaufman et al., 2002; Dubovik et al., 2021a). Therefore, the development and generation of long-term, high-quality and consistent atmospheric aerosol data records become crucial for the community to better understand aerosol effects on climate and human health (Pöschl, 2005; Chin et al., 2009; Boucher et al., 2013). To address this objective, a number of satellite missions dedicated to aerosol observations are continuously developed by the National Aeronautics and Space Administration (NASA), the European Space Agency (ESA) and other leading international agencies.

The Ocean and Land Color Instrument (OLCI) on the Copernicus Sentinel-3A satellite (Donlon et al., 2012) was launched on 16 February 2016 and its twin satellite Sentinel-3B on 25 April 2018. OLCI is the follow-on mission to the Medium Resolution Imaging Spectrometer (MERIS) instrument flown on ESA/Envisat (Rast et al., 1999; Donlon et al., 2012). The OLCI instrument is a medium-resolution and multi-spectral imager covering bands ranging from the visible to the far near-infrared. The primary operational applications are the ocean & land color monitoring for marine and land expert communities (Sentinel-3 OLCI User Guides, 2022). However, OLCI observations could also be used for obtaining valuable information for atmospheric aerosol characterization. Mei et al. (2018) showed 1st experiments by retrieving aerosol optical depth (AOD) from OLCI/Sentinel-3A instrument based on the XBAER algorithm for one month data (December 2016) during the haze episode. First results identified a positive bias potentially due to the cloud contamination. Today, Near-Real Time (NRT) aerosol retrieval from Sentinel-3 Sea & Land Surface Temperature Radiometer (SLSTR) has already been achieved by the European Organization for the Exploitation of Meteorological Satellites (EUMETSAT), with regular evolutions deployed in its ground-segment, entrusted by its European Commission mandate (https://www.eumetsat.int/atmospheric-composition;https://www.eumetsat.int/S3-AOD). This product is prepared to be operationally assimilated by the Copernicus Atmospheric Monitoring Service (CAMS). No global aerosol product is yet operational from OLCI in spite of its non-negligible atmospheric information content. Only the Level 2 (L2) Ocean Color processor, led by EUMETSAT, derives aerosol properties in the Near Infrared (NIR) over marine surfaces at the native OLCI resolution, for the sole purpose of atmospheric correction. Nevertheless, EUMETSAT is currently leading new activities to characterize and demonstrate the potential of retrieving a global AOD that would bring further information or new ideas to improve its current Sentinel-3 L2 processors.

The GRASP (Generalized Retrieval of Atmosphere and Surface Properties) algorithm was originally developed to exploit the aerosol information content from the Polarization and Directionality of the Earth's Reflectances (POLDER) multi-angular multi-spectral polarimetric (MAP) measurements (Dubovik et al., 2011, 2014, 2021b). GRASP is an algorithm of new generation and can in principle be applied to diverse passive and active remote sensing observations obtained from both down-looking satellite/airborne or up-looking ground-based observations (Lopatin et al., 2013, 2021; Benavent-Oltra et al., 2017, 2019; Torres et al., 2017; Li et al., 2019, 2022; Puthukkudy et al., 2020; Torres and Fuertes, 2021; Zhang et al., 2021). GRASP also was successfully used for interpretation of in situ and laboratory observations (Espinosa et al., 2017, 2019; Schuster et al., 2019). GRASP has a number of original features that often help accuracy or scope of the retrieval. For example, the first enhanced aerosol and surface product was obtained from POLDER multi-angular polarimetric observations (Dubovik et al., 2011). The extensive evaluation of POLDER/GRASP aerosol products by Chen et al. (2020) showed that the AOD retrieval performance is comparable with the single-viewing Moderate resolution Imaging Spectroradiometer (MODIS) AOD product, besides, the detailed aerosol properties, e.g. Ångström exponent (AE), fine/coarse mode AOD, aerosol absorption optical depth (AAOD), single scattering albedo (SSA), are of better quality from POLDER/GRASP. GRASP algorithm is designed to derive aerosol and surface properties simultaneously, as much as possible, to ensure the consistency of the products. The modular forward aerosol and surface modeling used in GRASP makes it flexible to optimize the algorithm for the different application purposes (Dubovik et al., 2021b). GRASP algorithm has also been or being applied for processing space-borne instruments of less information content comparing to POLDER-like multi-angular polarimeter measurements, such as MERIS and the Advanced Along-Track Scanning Radiometer (AATSR) onboard the Envisat satellite, the Tropospheric Monitoring Instrument (TROPOMI)/Sentinel-5P, the Second Generation Global Imager (SGLI)/GCOM-C, Himawari, etc. (Dubovik et al., 2021b). With support from ESA, the 11 years (2002−2012) MERIS/GRASP aerosol product (V1.1) has been released on the GRASP-OPEN website (http://www.grasp-open.com/products/meris-data-release/). There are ongoing efforts that are improving the current MERIS/GRASP product.

Thus, at present GRASP can be considered as a unified approach and software platform that is fully or partially portable for processing diverse types of remote sensing observations. This study describes the development of OLCI/Sentinel-3A aerosol and surface characterization based on the GRASP algorithm. The created dataset is available publicly from GRASP-OPEN (http://www.grasp-open.com/products/olci-data-release/) and the project description is on EUMETSAT (https://www.eumetsat.int/science-studies). Despite OLCI/Sentinel-3A and OLCI/Sentinel-3B sharing the same design, they do not have exactly same spectral characterization, radiometric and geometric calibrations (Lamquin et al., 2020). The present study is focused on the OLCI/Sentinel-3A, which at the time of this activity, was spectrally & radiometrically better characterized than its twin OLCI-B. The retrieval development is expected to be extended to process OLCI/Sentinel-3B in the future. A description of the OLCI/Sentinel-3A data preparation for retrieval is presented in Section 2, and the adaptation of the GRASP algorithm for OLCI aerosol and surface retrieval is presented in Section 3, followed by an evaluation of the derived aerosol and surface products in Section 4. In Section 5, we discuss some issues of the current baseline and evaluate the diagnosed detailed aerosol properties (e.g. AE and SSA). The summary and conclusion are considered in Section 6.

2. OLCI/Sentinel-3A instrument and data preparation

The Sentinel-3A is on a near-polar, sun-synchronous orbit with a descending node equatorial crossing at ~10:00 a.m. Local Time (LT). The OLCI instrument relies on a push-broom CCD technology to acquire Earth's TOA radiance in the solar spectral range from 400 nm to 1040 nm. OLCI has a 68.5° field of view around nadir and covers a swath of 1270 km (Sentinel-3 OLCI User Guides, 2022). Table 1 summaries the OLCI/Sentinel-3A spectral channels used for aerosol and surface characterization in this study. Fig. 1 shows the flow chart of the data preparation. Firstly, the OLCI/Sentinel-3A Level-1B (L1B) data are pre-processed through 4 steps (radiance normalization, pixel filtering, radiance correction, re-griding). The outputs are then archived in the GRASP multi-pixel segments (see Dubovik et al., 2011), which are the key inputs for GRASP aerosol-surface retrievals.

Step 1. The radiance normalization follows the scheme in Eq. (1):

$$\rho_{norm} = \frac{\rho_{TOA} \times \pi}{Flux} \quad (1)$$

Table 1
OLCI/Sentinel-3A spectral channels for aerosol and surface characterization in this study.

OLCI Band	Oa02	Oa03	Oa04	Oa05	Oa06	Oa08	Oa12	Oa17	Oa21
Central Wavelength (nm)	412.5	442.5	490	510	560	665	753	865	1020
Band Width (nm)	10	10	10	10	10	10	7.5	20	40
Radiometric Bias Correction	−2%	−2%	−2%	−2%	−2%	−2%	−2%	−2%	−6%

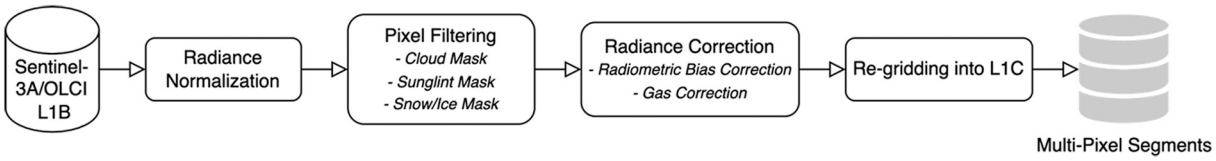

Fig. 1. Flow chart of the preparation of OLCI/Sentinel-3A L1B data to GRASP input multi-pixel segments.

where ρ_{norm} indicates the sun-normalized radiance, ρ_{TOA} is the L1B TOA radiance, and the solar flux (*Flux*) is adopted from the OLCI L1B metadata, which are already corrected for the Earth-Sun distance.

Step 2. The pixel filtering is done at OLCI L1B native resolution. In this study, we use L1B reduced resolution product, which is approximate at 1.2 km. The identification of pixel of properties (IDEPIX) processor (SNAP, 2022) is used to create the mask and filter cloud, sun-glint, and snow/ice contaminated pixels. The IDEPIX is an open-source SNAP processor developed by the Brockmann Consult GmbH (https://www.brockmann-consult.de/portfolio/idepix/) based on a neural network approach to calculate pixel-by-pixel classifications and cloud probability.

Step 3. The radiance correction consists of two parts: radiance radiometric bias correction and gas correction. Various radiometric validation exercises led by the Copernicus S3 Mission Performance Centre (S3MPC) produced by ESA, EUMETSAT, Sentinel-3 validation Teams (S3VT) overall demonstrate that OLCI-A absolute radiometric calibration has a positive brightness bias of about 2 to 3% throughout all the spectral bands, with the exception of band Oa21 (1020 nm) at about 6% (OLCI L1B user product notice - https://www.eumetsat.int/media/48140). Consequently, we follow the EUMETSAT's recommendations (informal communication) to correct the L1B radiances by −2% (Oa1-Oa20) and −6% (Oa21) from blue to near infrared channels (see in Table 1). The gas correction scheme, which was provided by the Free University of Berlin, is based on advanced K-distribution approach with k-bins components calculated for selected OLCI wavelengths (Doppler et al., 2014). The normalized column for water vapor and ozone are taken from the meteorology forecast, produced by the European Centre for Medium-Range Weather Forecasts (ECMWF), and made available in a timely manner together in the OLCI L1B product package. The contribution of nitrogen dioxide NO_2 is discarded as there is no corresponding value available in the L1B products.

Step 4. After the radiance normalization, pixel filtering and radiance correction, we then re-grid the pixels into L1C 10 × 10 km^2 spatial resolution under sinusoidal projection. The L1C are considered as valid if no >80% of the original L1B pixels were filtered out previously. To adapt the multi-pixel scheme, the L1C data are stored as 2 × 2 × NT segments for GRASP processing. Practically, we process season by season, therefore NT is the number of time layer for a 2 × 2 pixels' area over a particular season.

3. Application of GRASP algorithm for OLCI/Sentinel-3A aerosol and surface retrieval

The OLCI/GRASP retrieval baseline was initially adapted based on the implementation on the MERIS/GRASP retrieval that is implemented as solution realized in the frame of multi-term Least Square Method (LSM) methodology that allows simultaneous use of different a priori constraints (Dubovik et al., 2021b). Spectral dependent full BRDF parameters are directly retrieved together with 4 aerosol model relative concentrations and 1 aerosol total concentration. By assuming external mixture of aerosol components/models, aerosol single scattering characteristics are presented as a linear combination of 4 climatological models (smoke, urban, oceanic and dust). This method is known as GRASP/Models approach, which is described in detail by Chen et al. (2020), Lopatin et al. (2021) and Dubovik et al. (2021b). Specifically, the solution is sought as statistically optimized "multi-pixel" fitting realized via minimization of the quartic function defined for a large group of N (2 × 2 × NT) satellite pixels:

$$\boldsymbol{\Psi}(\boldsymbol{a}) = \sum_{i=1}^{N}\left[\left(\boldsymbol{f}_i(\boldsymbol{a}_i) - \boldsymbol{f}_i^*\right)^T \mathbf{W}_i^{-1}\left(\boldsymbol{f}_i(\boldsymbol{a}_i) - \boldsymbol{f}_i^*\right) + \boldsymbol{a}_i^T \boldsymbol{\Omega}_{single}\boldsymbol{a}_i\right] + \boldsymbol{a}^T \boldsymbol{\Omega}_{inter}\boldsymbol{a}, \quad (2)$$

$$\boldsymbol{\Omega}_{single} = \sum\nolimits_{i=1}^{N} \gamma^2 \boldsymbol{\Omega}_i, \quad (3)$$

$$\boldsymbol{\Omega}_{inter} = \gamma_x^2 \boldsymbol{\Omega}_x + \gamma_y^2 \boldsymbol{\Omega}_y + \gamma_t^2 \boldsymbol{\Omega}_t, \quad (4)$$

where $\boldsymbol{f}_i$ – vector of OLCI measurement logarithms in i-th pixel, $\boldsymbol{a}_i$ – vector of the retrieved parameters (logarithms of unknowns) for i-th pixel that includes both parameters of aerosol and surface reflectance, $\mathbf{W}_i$ – weighting matrix of the observations in the i-th pixel, $\boldsymbol{a} = (\boldsymbol{a}_i^T; \boldsymbol{a}_2^T; \ldots \boldsymbol{a}_N^T)^T$ - vector of unknows for N pixels. The second term in Eq. (2) includes so-called "single-pixel" smoothness constraints that limit variability of retrieved parameters within each pixel, and the degree of "single-pixel" smoothness constraints is adjusted by the "single-pixel" Lagrange multiplier γ (Eq. 3). While third term in Eq. (2) includes so-called "inter-pixel" constraints that limit the variability of retrieved parameters between pixels, and the degree of "inter-pixel" constraint is subject to the spatial and temporal Lagrange multiplier (γ_x, γ_y, γ_t) (Eq. 4). Following the idea of Dubovik et al. (2011) the OLCI/GRASP and MERIS/GRASP retrievals use the "single-pixel" smoothness constraints on spectral variability of BRDF parameters of land and ocean surfaces, and the limitations on temporal and spatial variability of BRDF parameters are used as "inter-pixel" constraints (the constraints on temporal variability of land BRDF are especially strong). Also, the temporal and spatial smoothness constraints are applied on the relative concentration of aerosol components ("models"): $c_i/(c_1 + c_2 + \ldots, c_N)$ (specifically 4 aerosol models in this study) that allowed to limit variability of the retrieved aerosol type. The summary of the inter-pixel constraint are discussed below in the Section 3.3 and all other general details of the formalism are provided in the papers by Dubovik et al. (2011, 2021b).

At the same time, OLCI observations are not fully identical to MERIS. Also, during last several years, GRASP approach and software have evolved and significant experience on practical processing of satellite and generally remote sensing measurements have been accumulated. Therefore, as an attempt of achieving the best OLCI retrieval accuracy,

some updates were incorporated into OLCI/GRASP retrieval setup (see in Sections 3.1 and 3.2). In this regard, it should be noted that the generated baseline processing OLCI/GRASP AOD results show solid consistency with ground-based Aerosol Robotic Network (AERONET) observations (Holben et al., 1998), yet the main shortcoming has been identified in presence of an essential bias (~0.1) at low AOD (550 nm) (<0.2). Thus, below we describe an important exercise carried out in order to specify the most optimal GRASP configuration baseline in view of a highly performant AOD (550 nm) from mono-viewing OLCI-like instrument. On top of that, we try to anticipate the AOD (550 nm) quality to meet as much as possible the operational scientific needs. For that purpose, a broad range of physics retrieval tests was applied. In this respect, the initial retrieval configuration ported from MERIS/GRASP is considered as the initial retrieval set up and the starting point for retrieval tuning and this base configuration was named as "Test 0". It should be noted that since MERIS didn't have the 1020 nm channel, the OLCI 1020 nm channel measurements were not included in the baseline Test 0 OLCI/GRASP retrieval.

The following tests are aimed to align optimally the OLCI/GRASP AOD and surface retrieval with the fundamental information content of the OLCI TOA radiance measurements. Furthermore, the key goal is highly on AOD (550 nm) performance to satisfy EUMETSAT operational scientific requirement. Other aerosol and surface parameters are of interest but not a key requirement. The proposed tests are focused on several specific aspects addressing issues specific for different observational situations. For example, aerosol retrieval difficulties are quite different over ocean and land surfaces. Therefore, some investigations are separated per surface cover type. At the same time, some of the research investigations and activities, such as the optimization of used spectral information, using rather general a priori constraints on retrieved aerosol parameters, optimization of radiative transfer (RT) calculations, etc. are relevant to retrievals at global scale and are performed in a coordinated approach. Table 2 provides an overview on the test cases planned and the details of the tests will be later discussed in the Section 3.1 (ocean) and Section 3.2 (land).

Table 2
List of test scenario over land and ocean surfaces.

Surface	Test ID[1]	Thematic	Experiment	Auxiliary Data
Ocean	1	Constraining angular properties of ocean surface BRDF	Fixed BRDF 2 and 3 A-Priori BRDF 2 and 3	ECMWF wind speed
	2	Optimizing the use of spectral OLCI data	OLCI Channel Weighting OLCI Channel Exclusion OLCI Channel + Outcome Test 1	
	3	Exploring the potential use of OLCI 1020 nm channel	Include 1020 nm Include 1020 nm + Outcome Test 2	
Land	4	Constraining angular properties of land surface BRDF	Fixed BRDF 2 and 3 A-Priori BRDF 2 and 3	POLDER-3/ GRASP surface climatology
	5	Optimizing the constraints for all parameters of land surface BRDF	Fixed All BRDF A-Priori All BRDF All BRDF + Outcome Test 4	
	6	Exploring the potential use of OLCI 1020 nm channel	Include 1020 Include 1020 + Outcome Test 5	

[1] Note that Test 0 is the starting point for a broad range of physics retrieval tests (Tests 1–6). Test 0 configuration is ported from MERIS/GRASP configuration.

In order to make quantitative and realistic evaluation of OLCI/GRASP performance, the tests were conducted with OLCI data collected over 16 AERONET ocean/coastal sites and 18 AERONET land sites, and all of them are selected according to their surface and/or aerosol type representativeness. The OLCI observations in 2 × 2 × NT (2 by 2 pixels for NT time layers) segments data centered over these AERONET sites are adopted in the tests. In order to test over pure ocean surface, we manually moved the selected ocean/coastal sites maximum ±0.3° latitude or longitude to use the OLCI measurements over ocean surface. Fig. 2 shows the spatial distribution of selected AERONET sites. The selection of AERONET sites is based on several principles:

a. to provide good global spatial coverage with sufficient data amount during 2018 to 2019
b. to provide good representation of various aerosol types
c. to provide a coverage of different land cover types for the retrieval tests over land and a sufficient dynamic of typical wind speed for ocean tests

To perform matchup of OLCI/GRASP test retrievals with AERONET, the AERONET Version 3 Level 2 direct-sun AOD (Smirnov et al., 2000; Giles et al., 2019) are averaged within ±30 mins of the OLCI/Sentinel-3A overpass. We filter the most reliable OLCI/GRASP retrievals using "residual relative" $= \sum_{i=1}^{N}\left[\left(\boldsymbol{f}_i(\boldsymbol{a}_i)-\boldsymbol{f}_i^*\right)^T\mathbf{W}_i^{-1}\left(\boldsymbol{f}_i(\boldsymbol{a}_i)-\boldsymbol{f}_i^*\right)\right]/N_{meas}$ (the first term in Eq. 2), where $\boldsymbol{f}_i^*$ and $\boldsymbol{f}_i(\boldsymbol{a}_i)$ represent measured and modelled TOA radiances, and N_{meas} is the number of measurements over wavelength and geometry. Here we used "residual relative" threshold 0.1 over ocean and 0.01 over land (indeed radiances over dark ocean surface have very low values, and relative fitting errors are generally much higher). The mean AOD over 2 × 2 OLCI/GRASP pixels is adopted, and we further examine the standard deviation of the mean and filtered standard deviation >0.05 over ocean and >0.1 over land. The matchup methodology has been kept consistent for all the tests in the Section 3.

Fig. 3 shows the validation of OLCI/GRASP baseline Test 0 AOD 550 nm results over selected 16 AERONET ocean sites and 18 AERONET land sites. The correlation is around 0.8 over ocean and 0.74 over land, with around 20.9% retrievals over ocean and 24.7% retrievals over land satisfying the Global Climate Observing System (GCOS) requirements: max (0.04 or 10%AOD). Note that the original definition of GCOS is max (0.03 or 10% AOD), while here we assume 0.01 uncertainty of AERONET direct sun AOD following the Aerosol_cci study by Popp et al. (2016) and POLDER validation by Chen et al. (2020). The main shortcoming of retrieval observed in the Test 0 is the bias for low AOD conditions ($BIAS_{AOD<0.2}$), which are around 0.11 over ocean and 0.09 over land respectively. These statistic metrics are close to one for the global evaluation based on the baseline processing that confirms the representative of selected AERONET sites for further tests.

3.1. OLCI/GRASP retrieval tests over ocean

The GRASP ocean surface BRDF model (e.g., see Dubovik et al., 2011, 2021b) utilizes the widely used Cox-Munk model (Cox and Munk, 1954) based on statistics of the sun's glitter on the sea surface in terms of the statistics of the slope distribution. Specifically, the OLCI/GRASP retrieval is relying on the following three-parameter approach:

$$R = \delta_{Fr}\left(a_{iso}(\lambda) + R_{CoxMunk}\left(\sigma^2\right)\right) + (1-\delta_{Fr})a_{foam}(\lambda) \quad (5)$$

where $a_{foam}(\lambda)$ is foam/whitecaps albedo with prescribed spectral dependence (Frouin et al., 1996; Frouin and Pelletier, 2015), $R_{CoxMunk}$ is the reflectance described by Cox-Munk model (Cox and Munk, 1954; Mischenko and Travis, 1997). The first parameter $a_{iso}(\lambda)$ denotes isotropic water leaving reflectance, the second parameter δ_{Fr} denotes the fraction of surface which provides Fresnel reflection (free from foam, dense sediments, whitecaps etc.), the third parameter σ denotes the

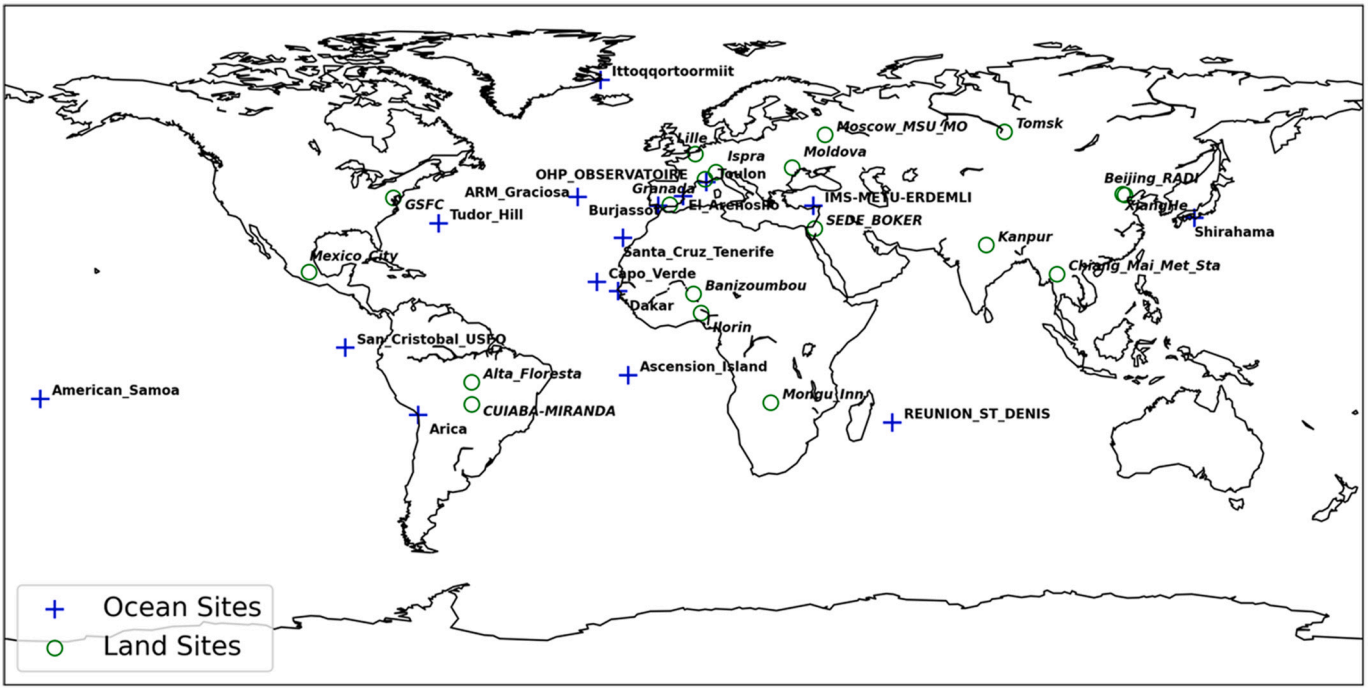

Fig. 2. Distribution of selected AERONET sites for OLCI/GRASP land and ocean retrieval tests.

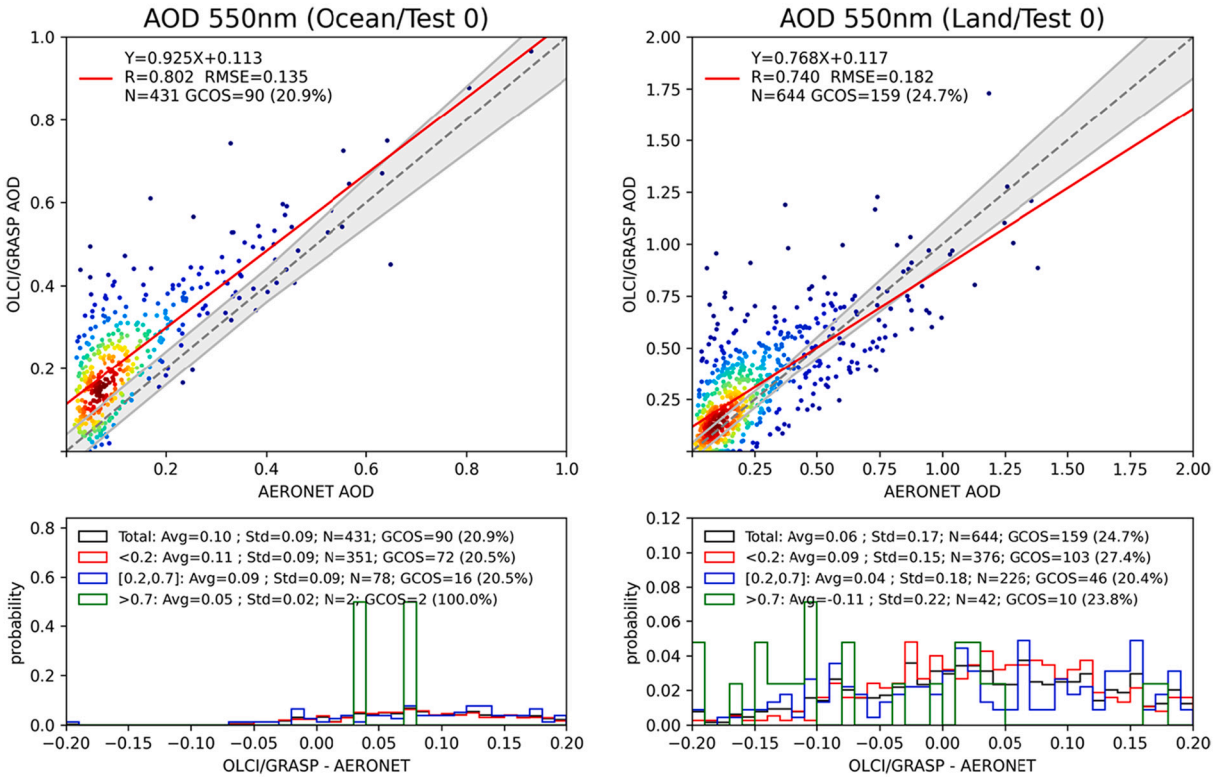

Fig. 3. Validation of OLCI /GRASP (Test 0) AOD 550 nm over selected AERONET land and ocean sites. The gray dashed line and the red solid line are the 1:1 reference line and the linear regression line. The gray envelope indicates GCOS requirement: max (0.04 or 10%AOD). The probability density functions of differences (OLCI-A/GRASP-AERONET) are present in the lower panel. The black, red, blue and green solid lines indicate all AOD conditions: any AOD, AOD < 0.2, $0.2 \leq$ AOD ≤ 0.7 and AOD > 0.7, respectively. (For interpretation of the references to color in this figure legend, the reader is referred to the web version of this article.)

mean square facet slope. In the OLCI/GRASP Baseline/Test 0 approach, all three parameters are retrieved using some minor a priori constraints on spectral ("single-pixel"), as well as, on spatial and temporal variability ("inter-pixel") of these parameters. Namely, five aerosol parameters (the relative concentrations of aerosol components and total aerosol concentration), eight values of $a_{iso}(\lambda)$, are retrieved together with δ_{Fr} and σ from eight measured values of OLCI TOA radiances. Certainly, some spectral smoothness ("single-pixel") constraints are applied on $a_{iso}(\lambda)$ (the limitation of first derivatives, with Lagrange parameter of 0.01–0.001), as well as, some minor smoothness constraints are applied on ("inter-pixel") temporal (the limitation of first derivatives, with Lagrange parameter of ~0.001) and spatial (the limitation of first derivatives, with Lagrange parameter of ~0.01) of all retrieved parameters and therefore the effective number of the retrieved parameters is evidently reduced. Nonetheless, a reasonable concern can be raised if such an extended set of unknowns can be uniquely retrieved from OLCI observations. Therefore, a number of tests have been suggested and planned in order to optimize the balance between retrieval and OLCI observation information content.

o Test 1: Constraining angular properties of ocean surface BRDF

Since OLCI is a mono viewing instrument, the OLCI TOA measurements have no or very limited sensitivity to angular features of BRDF. Therefore, a reliable retrieval of δ_{Fr} and σ can hardly be expected even if some a priori constraints of variability of these parameters were used. In this regard, in conventional satellite retrievals (i.e. MODIS, Levy et al., 2013), the angular properties of BRDF are commonly assumed using the ancillary knowledge of wind speed using known empirical relationships of the surface wind speed with δ_{Fr} and σ. Thus, the Test 1 is focused on verifying the effect of constraining the angular properties of water surface using this approach. Specifically, the following equations were used for defining δ_{Fr} and σ (Cox and Munk, 1954; Monahan and O'Muircheartaigh, 1980; Koepke, 1984; Frouin and Pelletier, 2015):

$$\delta_{Fr} = 1.0 - \left(2.95 \times 10^{-6} \times w^{3.52}\right) \quad (6)$$

$$2\sigma^2 = 0.003 + 0.00512 \times w \quad (7)$$

where w is the wind speed (unit: m/s) at the boundary layer, which is accessible in OLCI L1B data and is originally from ECMWF reanalysis dataset.

Therefore, the 2 experiments were done for constraining 2nd and 3rd parameters of water surface BRDF:

(i) The δ_{Fr} and σ^2 were not retrieved but fully fixed using the Eqs. (6) and (7) and ECMWF wind speed values;
(ii) δ_{Fr} and σ^2 were retrieved but using a priori estimates of the δ_{Fr} and σ^2 based on the Eqs. (6) and (7) and ECMWF wind speed values. In this case, the significantly high corresponding Lagrange parameters (e.g. 0.1) were applied (see discussions in Dubovik et al., 2011, 2021b).

The use of wind speed to constrain angular BRDF 2nd and 3rd parameters in Test 1 showed significant improvements in the retrieval: the R outcome from Test 1 improved significantly from 0.8 (Test 0) to be higher than 0.9, and the BIAS decreased to ~0.07 (see in Table 4). It should be noted that the difference between 2 experiments in Test 1 (fixed or a priori constrain on BRDF 2nd and 3rd parameters) was minor (the outcome of a priori constrain is slightly better in terms of validation metrics over test sites), therefore it is possible to conclude that the fixing δ_{Fr} and σ^2 or constraining the values to a priori estimates did not generate significant differences in AOD retrieval. Nonetheless, the retrieval of δ_{Fr} and σ^2 constrained by a priori estimates seemed to be a more flexible approach. Hence, the use of a priori estimates for δ_{Fr} and σ^2 is adopt as the outcome of Test 1 and will be used in the combination of next tests.

o Test 2: Optimizing the use of spectral OLCI data

Test 2 was aimed on optimizing the use of the OLCI observations at short wavelengths (412.5, 442.5, and 490 nm channels). In fact, the water leaving radiances in this spectral range depend on many factors (e.g., concentrations of chlorophyll or other soluble matters in the water) and, therefore higher uncertainty in water reflectance in these channels may cause higher uncertainty in AOD retrievals. This is a reason, why the most algorithms developed for mono- and bi-viewing sensors avoid the use of measurements at wavelengths lower than 550 nm over ocean surface (e.g. MODIS, SeaWiFS, VIIRS, etc.) (Remer et al., 2005; Sayer et al., 2012, 2018). Therefore, the Test 2 was designed to check if the high bias in OLCI/GRASP AOD could be related with a pronounced use of 412.5, 442.5, and 490 nm channels in the retrieval. At the same time, it is also clear that there is significant signal of aerosol at this shortwave spectral range and complete elimination of these channels may also waken the information content in the inverted data set. Thus, the tests were done with decreased weighting for short wavelengths or fully excluded measurements at short wavelengths. Some extra tests were also done by combining the ideas used in Tests 1 and 2, as well as by attempting to increase the constraints limiting variability of aerosol type, i.e. the relative presence of aerosol components in neighboring pixels. In addition, since GRASP algorithm has significant flexibility in inversion of observations, both possibilities of mentioned approaches, including the adjustment of the weights on the shortwave observations as well as a complete elimination of the channels from the retrievals were tested varying the fitting weights through increasing/decreasing the spectral channel noise (relative uncertainty) and strengths of used a priori constraints in the inversion. Specifically, the used combinations of the assumptions for the noise for each spectral channel is listed in Table 3.

Based on the output of Test 2 experiments, both the channel weighting and channel exclusion experiments showed some improvements with respect to the baseline Test 0 (no channel weight). At the same time, the complete elimination of short wavelength (412.5, 442.5 and 490 nm) measurements did not provide better results than using higher values for the noise assumed for the shorter wavelength measurements. Therefore, the channel weighting approach was chosen over complete elimination of these channels and adapted in all further tests. In addition, the combined ideas of Test 1 (a priori estimates for δ_{Fr} and σ^2), Test 2 (channel weighting) and introduced stronger inter-pixel constraints on aerosol type variability in spatial (X, Y) and temporal (T) dimensions showed some improvements (Outcome Test 2 in Table 4). Table 6 summarizes the single-pixel and inter-pixel constraints applied on the aerosol and surface characteristics. Specifically, the obtained AOD 550 nm showed R higher than 0.9, the BIAS is ~0.06, most importantly the GCOS fraction improved from ~30% (Outcome Test 1) to >40% (Outcome Test 2).

o Test 3: Exploring the potential use of OLCI 1020 nm channel

One of the potential advantages of the OLCI instrument compared to its predecessor MERIS is the addition of a longer wavelength at 1020 nm. The ocean surface is nearly black at this channel, including over optically complex waters (i.e. waters with heavy load of sediments) and most of the contribution to TOA observations comes from aerosols (if any) especially from coarse mode. Test 3 was designed to explore the potential use of 1020 nm OLCI channel. Note the OLCI/Sentinel-3A radiometric bias correction used for 1020 nm is −6%, while it is −2% for the other channels (see in Table 1).

The initial attempts of using OLCI 1020 nm channel measurements did not bring major changes of the AOD results, while some further adjustments of several retrieval assumptions appeared to be fruitful. Specifically, due to the wavelength range extended to 1020 nm, we need

Table 3
The channel noise (relative uncertainty) used in OLCI/GRASP ocean retrieval to achieve channel weight and channel exclusion.

	Channel Noise								
Wavelength (nm)	412.5	442.5	490	510	560	665	753	865	1020
No channel weight	0.01	0.01	0.01	0.01	0.01	0.01	0.01	0.01	0.01 (If used)
Channel weight	0.1	0.1	0.1	0.01	0.01	0.01	0.01	0.01	0.01 (If used)
Channel exclusion	1.0	1.0	1.0	0.01	0.01	0.01	0.01	0.01	0.01 (If used)

Table 4
Summary of AERONET validation statistic metrics of AOD 550 nm resulting from OLCI/GRASP ocean tests.

	R	RMSE	GCOS (%)	$BIAS_{TOTAL}$	$BIAS_{AOD<0.2}$	Num. of pairs
Baseline Test 0	0.802	0.135	20.9	0.10	0.11	431
Outcome Test 1	0.911	0.087	29.6	0.07	0.07	540
Outcome Test 2	0.902	0.081	41.3	0.06	0.06	542
Outcome Test 3	0.889	0.057	70.8	0.01	0.01	541

to adjust further the a priori smoothness constraints on spectral variability of $a_{iso}(\lambda)$ by using the derivatives of 1st order with Lagrange parameter of 0.001 (see in Table 6). Furthermore, the use of OLCI 1020 nm measurements in combination with the outcomes of Test 1 (using a priori estimates for δ_{Fr} and σ^2) and Test 2 (adjusting channel weighting) lead to the outcome of Test 3 that showed significant improvement: the R improved from 0.801 (Baseline Test 0) to 0.889 (Outcome Test 3), the GCOS fraction increased from 21.1% to 70.8%. The total bias ($BIAS_{TOTAL}$) decreased from 0.10 to 0.01, and the bias for low AOD ($BIAS_{AOD<0.2}$) decreased from 0.11 to 0.01. Finally, the all developments integrated from Test 1 to Test 3 demonstrated significant improvement for retrieval of AOD over ocean.

3.2. OLCI/GRASP retrieval tests over land

The GRASP land surface BRDF calculations used for OLCI are based on Ross-Li model (Ross, 1981; Li and Strahler, 1992):

$$BRDF_{Ross-Li} = a_{iso}(\lambda)\left[1 + a_{vol}f_{vol} + a_{geom}f_{geom}\right] \quad (8)$$

where $a_{iso}(\lambda)$ denotes isotropic term, a_{vol} denotes volumetric term and a_{geom} denotes geometrical term, f_{vol} and f_{geom} denote volumetric and geometric scattering kernels. The above formulation of Ross-Li model given by Eq. (8) was proposed by Litvinov et al. (2011a, 2011b). In difference with previous equations used for this model, the spectral dependence of BRDF is included only to $a_{iso}(\lambda)$. Also, based on the extensive analysis of observational data by Litvinov et al. (2011a, 2011b), the parameters a_{vol} and a_{geom} were considered spectrally independent. In baseline OLCI/GRASP AOD approach, eight values of $a_{iso}(\lambda)$ and two spectrally dependent parameters a_{vol} and a_{geom} are retrieved under rather strong constraints of temporal variability of these parameters. At the same time, the single viewing OLCI measurements seem to have a low sensitivity to angular features of BRDF that are described by volumetric and geometric terms in Eq. (8). Moreover, realistic separation of surface and aerosol contributions in satellite observation over land surface is generally a very challenging task. Therefore, a series of tests were proposed to optimize the separation aerosol and surface information in OLCI retrieval over land.

In order to conduct the tests using a priori estimate for surface reflectance, a monthly surface climatology was generated for 3 Ross-Li BRDF parameters from POLDER-3 GRASP/Optimized processing climatological dataset (https://www.grasp-open.com/products/polder-data-release/). To adapt the climatology for OLCI wavelengths, the interpolation and exploration were performed using the nearest POLDER-3 wavelengths. Note the current GRASP/Optimized climatological dataset is available from latitude 60°S to 60°N.

- Test 4: Constraining angular properties of land surface BRDF

Based on rather positive outcome from the ocean tests, we implemented 2 modifications to optimize the OLCI/GRASP baseline land configuration before performing Test 4:

(i) we introduced stronger inter-pixel constraints on aerosol type variability in spatial (X, Y) and temporal (T) dimensions (see Table 6);
(ii) we assumed explicitly the spectrally independent volumetric and geometric BRDF parameters (a_{vol} and a_{geom}) in the retrieval.

Similar to the Test 1 for ocean surface, two experiments were conducted over land in Test 4 to constrain angular properties of land surface BRDF:

(i) The parameters a_{vol} and a_{geom} were directly fixed using the POLDER-3/GRASP climatology;
(ii) A priori estimates of a_{vol} and a_{geom} were used from the POLDER-3/GRASP climatology with significantly high corresponding Lagrange multiplier parameters (e.g. 0.1).

In general, the optimized setting together with the constraint on the angular properties of land surface BRDF using climatology resulted in improved performance of the retrievals (Outcome Test 4 in Table 5). The correlation coefficient R improved from 0.740 (Baseline Test 0) to 0.834, the $BIAS_{AOD<0.2}$ decreased from 0.09 to 0.02. It should be noted that based on our tests, using the a_{vol} and a_{geom} from the climatology as a priori estimates helped to generate slightly better results than directly fixed them. Hence, the use of a priori estimates was adapted as selected approach for further tests.

- Test 5: Optimizing the constraints for all parameters of land surface BRDF

In the Test 5, we attempted to constrain BRDF isotropic term $a_{iso}(\lambda)$ using a priori estimates from the climatological values. The outcome of the test showed that in practice, using a priori estimates or fixing $a_{iso}(\lambda)$ from climatology did not help to improve the overall retrieval results,

Table 5
Summary of AERONET validation statistic metrics of AOD 550 nm resulting from OLCI/GRASP land tests.

	R	RMSE	GCOS (%)	$BIAS_{TOTAL}$	$BIAS_{AOD<0.2}$	Num. of pairs
Baseline Test 0	0.740	0.182	24.7	0.06	0.09	644
Outcome Test 4	0.834	0.142	29.4	0.03	0.04	591
Outcome Test 5	0.869	0.110	36.5	−0.02	0.00	646
Outcome Test 6	0.880	0.105	39.4	−0.02	0.00	625

sometimes lead to a significantly degraded convergence of OCLI measurement fitting. Therefore, we utilized the climatological values of $a_{iso}(\lambda)$ as an initial guess without applying any a priori constraint. In addition, it was found that using vector radiative transfer in forward model calculation, which was not planned originally (e.g. was not used in MERIS/GRASP processing), is also beneficial for improving retrieval performance. Finally, by optimizing the retrieval all three BRDF parameters using the climatology in Test 5 (using initial guess for isotropic term and a priori estimates for volumetric and geometric terms), we have observed the reduction of the $BIAS_{AOD<0.2}$ for low AOD from 0.09 (Baseline Test 0) to 0.00 (Outcome Test 5), the decrease of RMSE from 0.18 to 0.11 and an improvement of R from 0.74 to 0.87 (see Table 5).

o Test 6: Exploring the potential use of OLCI 1020 nm channel

A series of Tests 6 was designed to explore the potential effect from adding OLCI 1020 nm measurements into retrieval while integrating all advances identified in Tests 4 and 5. Comparing AERONET validation outcome for Test 6 results with that for Test 5 showed rather similar results with the only notable difference between the results of tests relevant to using or not 1020 nm channel. Namely, it was clear that some improvements can be observed for the GCOS fraction against AERONET that improved from 36.5% (Outcome Test 5) to 39.4% (Outcome Test 6).

This result suggested that the use of a 1020 nm channel is not crucial for improving AOD retrieval from OLCI especially for eliminating the biases over land. The positive effects from additional 1020 nm measurements are more pronounced over ocean than over land which is probably due to the fact that the aerosol over ocean is mainly coarse mode dominant. At the same time, several minor but useful improvements were observed in the retrieval once 1020 nm observations were added. Therefore, using this channel was recommended for future processing taking also in account that the observations at longer wavelengths are overall helpful for separation of land surface contribution from aerosol. Indeed, while the contribution of underlying surface often dominates at longer wavelengths the observations at 1020 nm have extra sensitivity compared to other channels to coarse aerosols such as desert dust.

3.3. Summary of OLCI/GRASP land and ocean retrieval tests

This section described the efforts on implementing a large time-series of the retrieval tests of AOD from Sentinel-3A/OLCI over land and ocean. We performed >50 tests using different configurations of surface climatology, constraints, etc. As a result, the positive evolution of OLCI/GRASP AOD retrieval can be clearly seen through the test results from baseline Test 0 to Test 3 over ocean (Table 4) and Test 6 over land (Table 5).

Thus, based on the results of the retrieval tests over land and ocean, the optimized configurations for ocean and land OLCI/GRASP retrievals are determined:

- Ocean (Test 3):

  (i) the use of wind speed data for constraining angular ocean surface BRDF properties (using a priori estimates for δ_{Fr} and σ^2 calculated based on wind speed from ECMWF values);
  (ii) the assumption of higher measurement noise at short wave channels (412.5, 442.5, and 490 nm);
  (iii) the inclusion of OLCI 1020 nm measurements.

- Land (Test 6):

  (i) using the values obtained from POLDER-3/GRASP monthly surface climatology for initial guess of Ross-Li BRDF isotropic term $a_{iso}(\lambda)$, and for a priori estimates for volumetric and geometric terms (a_{vol} and a_{geom});
  (ii) the implementation of stronger constraints on aerosol type variability in spatial and temporal dimensions and the assumption of spectral independence of BRDF volumetric and geometric terms (a_{vol} and a_{geom});
  (iii) the inclusion of OLCI 1020 nm measurements;
  (iv) the utilization of vector radiative transfer in forward model calculation.

For OLCI/GRASP retrieval, the state vector of each land or ocean pixel can be written as:

$$\begin{aligned} \boldsymbol{a}_{i-land} &= \left[c_t, c_1/c_t, c_2/c_t, c_3/c_t, c_4/c_t, a_{iso}(\lambda), a_{vol}, a_{geom}\right]^T \text{ or} \\ \boldsymbol{a}_{i-ocean} &= \left[c_t, c_1/c_t, c_2/c_t, c_3/c_t, c_4/c_t, a_{iso}(\lambda), \delta_{Fr}, \sigma\right]^T, \end{aligned} \quad (9)$$

It is important to note that OLCI/GRASP derives rather extended set of parameters of each pixel: BRDF_1 at 9 wavelengths + BRDF_2 + BRDF_3 + 4 relative aerosol model concentrations (c_1/c_t, …, c_4/c_t) + 1 aerosol total concentration ($c_t = c_1 + c_2 + c_3 + c_4$) = 16 unknowns that is >9 OLCI measurements per pixel. Also, the retrieval used only 2 direct a priori estimates for BRDF_2 and BRDF_3. The handling such large number of unknowns in the state vector is only possible by using single-pixel and inter-pixel constraints that make applying some relationships in the parameters retrieved in different pixels and therefore reduce effective number of actually derived values. Table 6 summarize the details of single-pixel constraints and inter-pixel spatial and temporal constraints applied on the OLCI/GRASP land and ocean retrieval.

The outlined above optimized settings for the OLCI/GRASP retrieval are quite suitable for attempting to generate aerosol and surface products simultaneously in the fully consistent manner globally. Namely, both over land and ocean OLCI/GRASP retrieval uses all 9 spectral channels and exactly the same approach for modeling aerosol scattering (GRASP/Models approach). Due to the lack of angular information in single view satellite observations, the angular properties of underlying surface are strongly constrained in the retrieval: over ocean Fresnel reflection together with foam/whitecap albedo are constrained using its a priori estimates based on ECMWF wind speed, and over land BRDF retrieval is constrained using a priori estimates for Ross-Li volumetric and geometric terms obtained from POLDER surface climatology. Meanwhile, the isotropic reflectance is retrieved both over land and ocean under mild spectral smoothness constraints.

Fig. 4 shows the validation of OLCI/GRASP retrieved AOD 550 nm over selected sites by using Test 3 configuration for ocean and Test 6 configuration for land retrieval respectively. In comparison with the baseline Test 0 results in Fig. 3, the evolution can be clearly observed in all parameters of validation metrics. The most spectacular improvements are probably the reduction of biases for low AOD cases ($BIAS_{AOD<0.2}$) from ~ +0.10 to the values within ±0.01. The Test 3 and Test 6 configurations are then used for OLCI/GRASP global processing.

4. Evaluation of OLCI-A/GRASP aerosol and surface products

In order to evaluate the development of OLCI/GRASP retrieval on global scale, we processed one year (June 2018 to May 2019) data using the outcome configurations in Section 3 (Ocean: Test 3; Land: Test 6). The product is freely available from GRASP-OPEN website (https://www.grasp-open.com/products/olci-data-release/). Table 7 lists the aerosol and surface parameters in the OLCI/GRASP product. Please note relative concentrations of 4 aerosol models and total aerosol concentration are directly retrieved parameters (Eq. 9), and the spectral AOD, AAOD SSA and AE are derived from them. For surface, the BRDF parameters are directly retrieved (Eq. 9) and other surface characteristics, such as black-sky/white-sky albedos and Normalized Difference Vegetation Index (NDVI), are the derived products.

The generated OLCI/GRASP results were validated and evaluated in this section following a similar concept as used by Chen et al. (2020) for evaluating POLDER-3/GRASP retrieval. Correspondingly, the OLCI/

Table 6
Summary of detailed single-pixel spectral constraints and inter-pixel spatial and temporal constraints applied on the retrieved aerosol and surface characteristics.

Aerosol and surface characteristics	Single-pixel constraints		Inter-pixel constraints			
			Spatial constraints		Temporal constraints	
	Order of finite difference	Lagrange parameter	Order of finite difference	Lagrange parameter	Order of finite difference	Lagrange parameter
Relative concentration of aerosol models	–	–	1	1.0e-1	1	1.0e-2
Total aerosol concentration	–	–	1	- (Land) 1.0e-3 (Ocean)	1	- (Land) 1.0e-4 (Ocean)
Ross-Li isotropic term	1	1.0e-3	–	–	1	5.0
Ross-Li vol and geo terms	–	–	1	1.0e-4	–	–
Isotropic water leaving radiance	1	1.0e-3	–	–	1	5.0
Fresnel reflection and the facet slope	–	–	1	1.0e-4	–	–

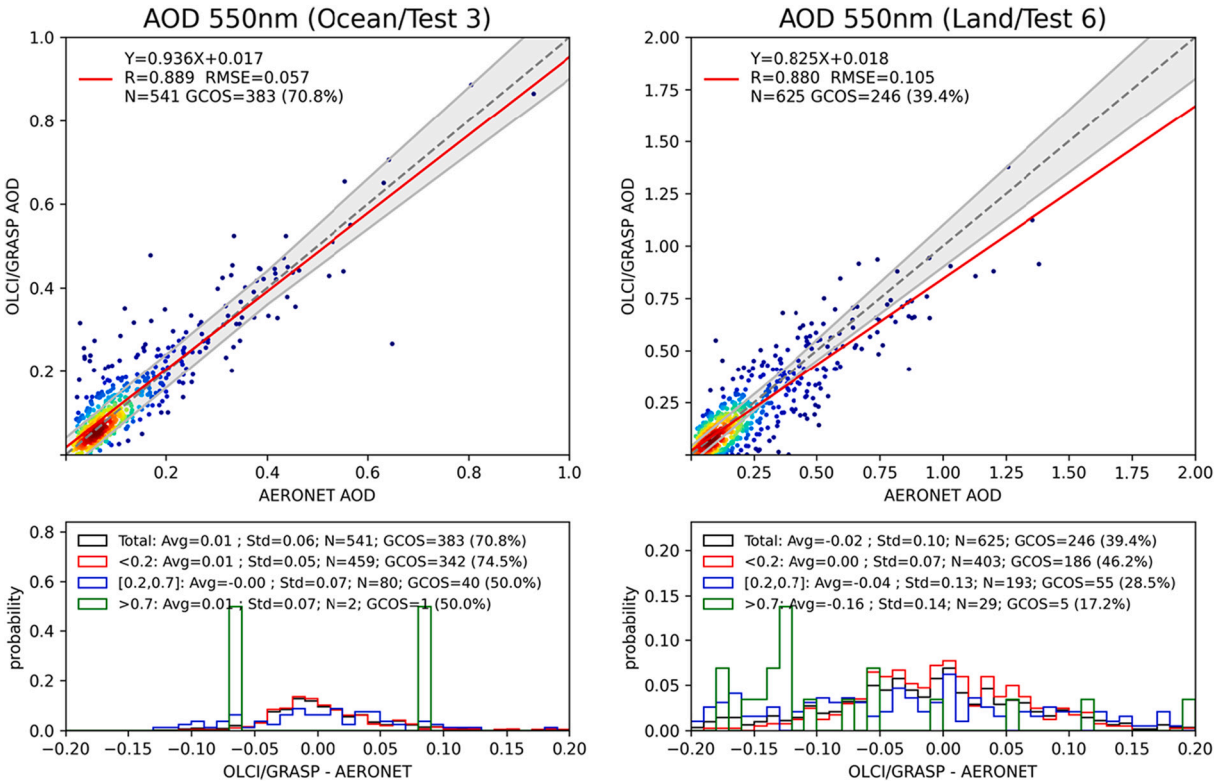

Fig. 4. Validation of OLCI/GRASP AOD 550 nm over selected AERONET land (Test 6) and ocean (Test 3) sites.

GRASP validation results were also compared with results of validation of MODIS retrieval performed for the same time period using the same validation approach. In addition, OLCI/GRASP retrieval were compared globally with MODIS products. All comparisons were done separately for observations over land and ocean. In addition, over ocean validation was also done separately for permanent coastal/island AERONET sites and MAN ship-borne measurements obtained mainly over deep ocean. Thus, the section contains the following materials:

- o The generated OLCI/GRASP global aerosol products validation against the AERONET Version 3 Level 2 direct-sun AOD reference dataset
- o The validation of MODIS/TERRA Collection 6.1 Dark Target + Deep Blue combined AOD products (Levy et al., 2013; Sayer et al., 2014) against AERONET both over land and ocean for the same period as OLCI/GRASP, and intercompared the obtained MODIS products evaluation statistics with OLCI/GRASP AERONET validation results
- o Validations of the products against the deep ocean AERONET - Maritime Aerosol Network (MAN) measurements (Smirnov et al., 2009), and intercomparison of validation results with MODIS products
- o Grided pixel-to-pixel inter-comparison of OLCI/GRASP and MODIS aerosol and surface products

4.1. *Aerosol validation against AERONET*

OLCI/GRASP and MODIS/TERRA Dark Target (DT) + Deep Blue (DB) combined aerosol products are at ~10 km spatial resolution. A matchup strategy of selecting satellite observations for validation with AERONET data was adapted from the work by Chen et al. (2020). Specifically, the gridded satellite retrievals were averaged in following windows centred over the AERONET station: 5 × 5 over land and 9 × 9 over ocean. Any adjacent pixels to land/ocean or land-ocean mixed pixels are omitted. The minimal 50% coverage of satellite pixels within a

Table 7
List of OLCI/GRASP aerosol and surface products and the parameters' description.

Category	Parameters	Description
Aerosol	AOD (λ)	spectral aerosol optical depth
	AAOD (λ)	spectral aerosol absorption optical depth
	SSA (λ)	spectral single scattering albedo
	AE	Ångström exponent
Surface	Ross_Li_BRDF_iso (λ)	isotropic term of Ross-Li BRDF
	Ross_Li_BRDF_vol	volumetric term of Ross-Li BRDF
	Ross_Li_BRDF_geo	geometric term of Ross-Li BRDF
	Cox_Munk_iso (λ)	isotropic water leaving radiance
	DHR (λ)	directional hemispherical reflectance (black-sky albedo)
	BHR_ISO (λ)	isotropic bihemispherical reflectance (white-sky albedo)
	NDVI	Normalized Difference Vegetation Index
Supplementary	ResidualRelative	relative fitting residual
	ResidualAbsolute	absolute fitting residual
	Latitude	-
	Longitude	-
	MASL	metres above sea level
	LandPercentage	Land percentage (%)

λ = 412, 442, 490, 510, 560, 665, 753, 865 and 1020 nm.

window is used as acceptance threshold. The AERONET direct-sun AOD products are averaged within ±30 mins of the OLCI/Sentinel-3A and MODIS/TERRA overpass time. Only the high-quality retrieval products for MODIS/TERRA (quality flag QA = 3 over land and QA ≥2 over ocean) were used. For OLCI/GRASP products, we require fitting relative residual (mean root square of relative error in fitting the measurements by the algorithm) <1% over land and 5% over ocean and the AOD 550 nm standard deviation within each window below than 0.1 over land and below of 0.05 over ocean.

Fig. 5 shows the validation results for AOD at 550 nm for OLCI/GRASP and MODIS/TERRA DT + DB combined product over land and ocean for one-year period June 2018 to May 2019. The OLCI/GRASP and AERONET AOD is interpolated to the reference wavelength 550 nm using AE (AE $= \frac{ln[\tau(\lambda_1)/\tau(\lambda_2)]}{ln(\lambda_2/\lambda_1)}$). Over land (Fig. 5a and c), the total matched points are 3205 for OLCI/GRASP and 12,632 for MODIS/TERRA DT + DB combined product. This difference in the matched points in OLCI and MODIS data sets is possibly due to the wider swath of MODIS (2330 km) than Sentinel-3 OLCI (1270 km) as well as due to the differences in the cloud screening. The obtained statistic metrics for 2 products are quite comparable, e.g., MODIS/TERRA (R = 0.889, RMSE = 0.115, GCOS = 49.3%) and OLCI/GRASP (R = 0.870, RMSE = 0.090, GCOS = 47.9%). In terms of bias, OLCI/GRASP ($BIAS_{TOTAL}$ = 0.01 and $BIAS_{AOD<0.2}$ = 0.01) is slightly better than MODIS ($BIAS_{TOTAL}$ = 0.02 and $BIAS_{AOD<0.2}$ = 0.02). However, as one of rather minor shortcoming of the OLCI/GRASP products, the apparent underestimation of high AOD cases corresponding to negative bias when AOD > 0.2 can be noted. This aspect needs to further investigations in future studies. One of the possible reasons is the too strict cloud screening, because the proportion of high AOD cases (AOD > 0.7) for OLCI/GRASP is 2.3% (73/3205) that is almost 1.6 times less than that of MODIS 3.8% (483/12632). Over ocean (Fig. 5b and d), MODIS/TERRA AOD show higher correlation (R = 0.955) than OLCI/GRASP (0.872), which maybe because of the missing of high AODs for OLCI/GRASP. For the other metrics of the statistics, OLCI/GRASP AOD product is slightly better than MODIS/TERRA, e.g., OLCI/GRASP: RMSE = 0.047, GCOS = 67.3%, $BIAS_{TOTAL}$ = 0.01 and $BIAS_{AOD<0.2}$ = 0.01, while for MODIS: RMSE = 0.050, GCOS = 66.3%, $BIAS_{TOTAL}$ = 0.02 and $BIAS_{AOD<0.2}$ = 0.03.

Table 8 summaries OLCI/GRASP spectral AOD products validation metrics against AERONET at 440, 550, 670, 865 and 1020 nm over land and ocean. Over land, the OLCI/GRASP shows good agreement with AERONET spectral AOD with R varying from ~0.8 (1020 nm) to 0.88

Table 8
Summary of statistics of OLCI/GRASP spectral AOD products against AERONET AOD at 440, 550, 670, 865 and 1020 nm over land and ocean.

	OLCI/GRASP spectral AOD products	R	RMSE	GCOS (%)	$BIAS_{TOTAL}$	$BIAS_{AOD<0.2}$
Land	AOD 440 nm	0.881	0.120	38.9	−0.02	0.02
	AOD 550 nm	0.870	0.090	47.9	−0.01	0.01
	AOD 670 nm	0.857	0.075	54.8	0.00	0.02
	AOD 865 nm	0.821	0.063	61.8	0.01	0.02
	AOD 1020 nm	0.798	0.060	62.6	0.02	0.02
Ocean	AOD 440 nm	0.893	0.064	52.1	0.02	0.03
	AOD 550 nm	0.872	0.047	67.3	0.01	0.01
	AOD 670 nm	0.902	0.038	76.1	0.01	0.02
	AOD 865 nm	0.866	0.031	82.8	0.00	0.01
	AOD 1020 nm	0.848	0.029	85.8	0.00	0.00

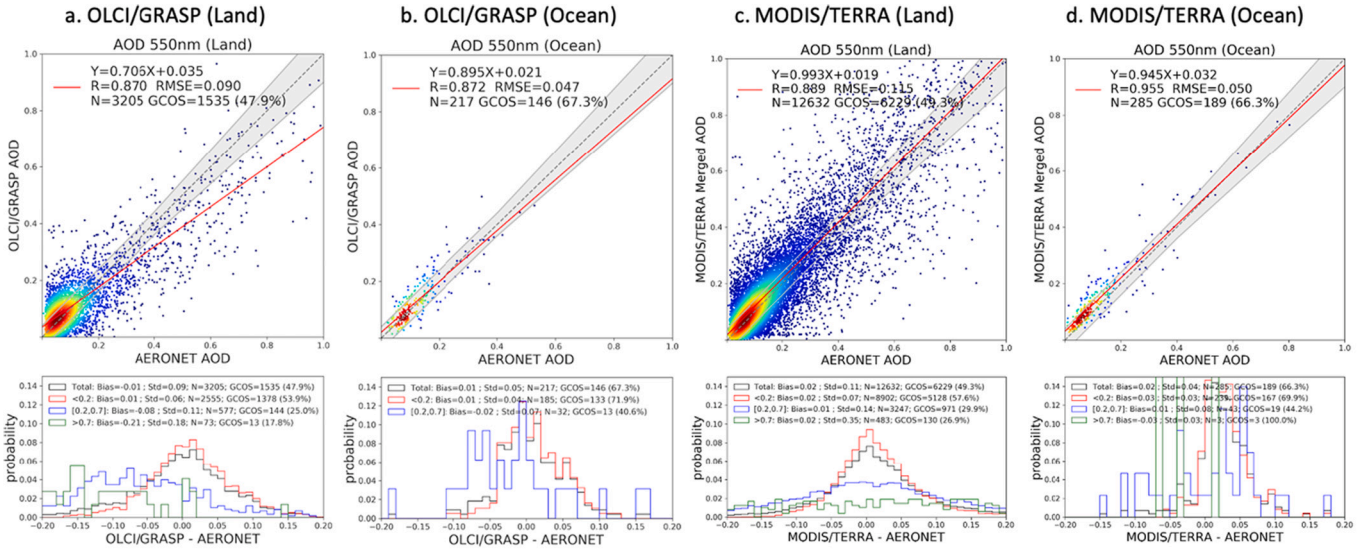

Fig. 5. Validation of one-year OLCI/Sentinel-3A GRASP and MODIS/TERRA DT + DB combined AOD 550 nm over land and ocean against AERONET Version 3 L2 direct sun AOD. (a). OLCI/GRASP AOD validation over land; (b). OLCI/GRASP AOD validation over ocean; (c). MODIS/TERRA DT + DB combined AOD validation over land; (d). MODIS/TERRA DT + DB combined AOD validation over ocean.

(440 nm), RMSE is smaller than 0.12 and GCOS is higher than 38.9% from blue to near infrared channels, and the BIAS is not exceeding ±0.02. Over ocean, the R is >0.84, and RMSE is smaller than 0.07 and GCOS is higher than 50% from blue to near infrared channels, as well as the bias within ±0.02.

In order to compare the performance over different land surfaces, the statistics of AOD validation against AERONET were generated separately for different Normalized Difference Vegetation Index (NDVI) values: bare soil/desert surfaces (NDVI<0.2), mixture of bare soil and vegetated surfaces (0.2 ≤ NDVI<0.4) and surfaces covered different types of vegetation (0.4 ≤ NDVI<0.6 and NDVI≥0.6). Fig. 6 shows the statistics for different NDVI land surfaces for 5 main parameters (R, RMSE, GCOS, $BIAS_{TOTAL}$, $BIAS_{AOD<0.2}$). Generally, both products are less accurate over bright surface (NDVI<0.2), where MODIS DT + DB combined AOD product is slightly more accurate than OLCI/GRASP. The bias for OLCI/GRASP is noneligible (0.05–0.06) for NDVI<0.2 that is higher apparently than the bias in MODIS (0.03–0.04). At the same time, in the range of 0.2 ≤ NDVI<0.4, where the surface is mixture of bare soil and vegetation, OLCI/GRASP AOD product seems more accurate than the MODIS/TERRA DT + DB combined AOD product. As for the other two categories (0.4 ≤ NDVI<0.6 and NDVI≥0.6), the two products show overall similar accuracy. Note the signs of BIAS for NDVI≥0.4 are opposite (MODIS: ~ +0.02; OLCI: ~–0.02).

In addition to the validation metrics generated for global data, we compared the validation metrics of OLCI/GRASP and MODIS/TERRA DT + DB combined aerosol products over spatially distributed AERONET sites. The AOD validation is conducted over all AERONET sites that have available data in the period June 2018 to May 2019. In order to make sure the statistics is robust, only sites with at least 10 matchup points are included in the analysis. In general, MODIS/TERRA DT + DB combined aerosol products cover more sites than OLCI/GRASP (274 vs. 112) where the 10 matchups threshold is reached. Fig. 7 shows the distribution of site validation metrics of OLCI (Fig. 7a) and MODIS (Fig. 7b). The size of the circle represents the number of matched points. Also, the differences (OLCI – MODIS) of metrics (R, RMSE, BIAS and GCOS) are presented in the right panel (Fig. 7c). Statistically, over co-covered sites, OLCI/GRASP AOD products show better agreement with AERONET than MODIS data over 36% sites for R, 62% sites for RMSE, 52% sites for BIAS and 48% sites for GCOS. In general, MODIS shows higher correlation coefficients, while OLCI/GRASP has lower values of RMSE. For the BIAS and GCOS fraction, the two products are quite comparable.

4.2. Aerosol validation against maritime aerosol network (MAN)

In addition to the validation of satellite data over ocean with AERONET permanent island and coastal sites, the data from AERONET Maritime Aerosol Network (MAN) (Smirnov et al., 2009, 2011) were used to evaluate OLCI/GRASP and MODIS/TERRA AOD over deep ocean. The MAN AOD measurements are performed in ships navigations continuously (non-stop) across all oceans and the strategy of data colocation needed some adjustments. Specifically, in order to simplify the colocation, the MAN Level 2 AOD were re-gridded into 0.1-degree grid box to make the data structure close to the OLCI/GRASP and MODIS 10 km aerosol products. In addition, the MAN AOD measurements are relatively rare, therefore we selected the satellite data within approximately the same day (± 360 mins) using the same 9 × 9 window, as was used in coastal sites validation. In addition, similar to AERONET ocean validation, we selected MODIS/TERRA AOD with QA ≥2 and OLCI/GRASP retrievals with relative residual <5% and AOD standard deviation within the 9 × 9 window smaller than 0.05.

Thus, we performed validation for OLCI/GRASP and MODIS/TERRA and the results of AOD 550 nm for a year (June 2018 to May 2019) are shown in Fig. 8. In general, OLCI/GRASP AOD (Fig. 8a) shows slightly better agreement with MAN measurements than MODIS/TERRA (Fig. 8b) in terms of statistic metrics. For example, for MODIS/TERRA we obtained: $R = 0.866$, RMSE = 0.061, GCOS = 61.1%, BIAS = 0.04 and for OLCI/GRASP: $R = 0.891$, RMSE = 0.045, GCOS = 74.2%, BIAS = 0.00. In general, the obtained MODIS statistic metrics against MAN are close to the recent MODIS team reported (Remer et al., 2020), and the observed positive biases in DT ocean AOD are largely assumed to be (i) the algorithm does not allow negative AOD retrieval over ocean, and (ii) the use of a spherical instead of spheroid model for dust particles (Lee et al., 2017; Zhou et al., 2020). Fig. 9 shows the differences of AOD 550 nm between MODIS/TERRA, OLCI/GRASP and MAN measurements. In general, MODIS/TERRA AOD is higher than MAN AOD globally (Fig. 9b) by a value of about 0.04. OLCI/GRASP (Fig. 9a), in general, has smaller bias than MODIS, while there are some cases over the Mid-Atlantic, where OLCI/GRASP AOD shows underestimations. Fig. 10 shows the OLCI/GRASP spectral AOD validation against MAN/AERONET measurements. From blue to NIR channels, the correlation coefficients are higher than 0.88, with RMSE 0.028 to 0.059, GCOS fraction 62.1% to 85.6%, and bias within ±0.01.

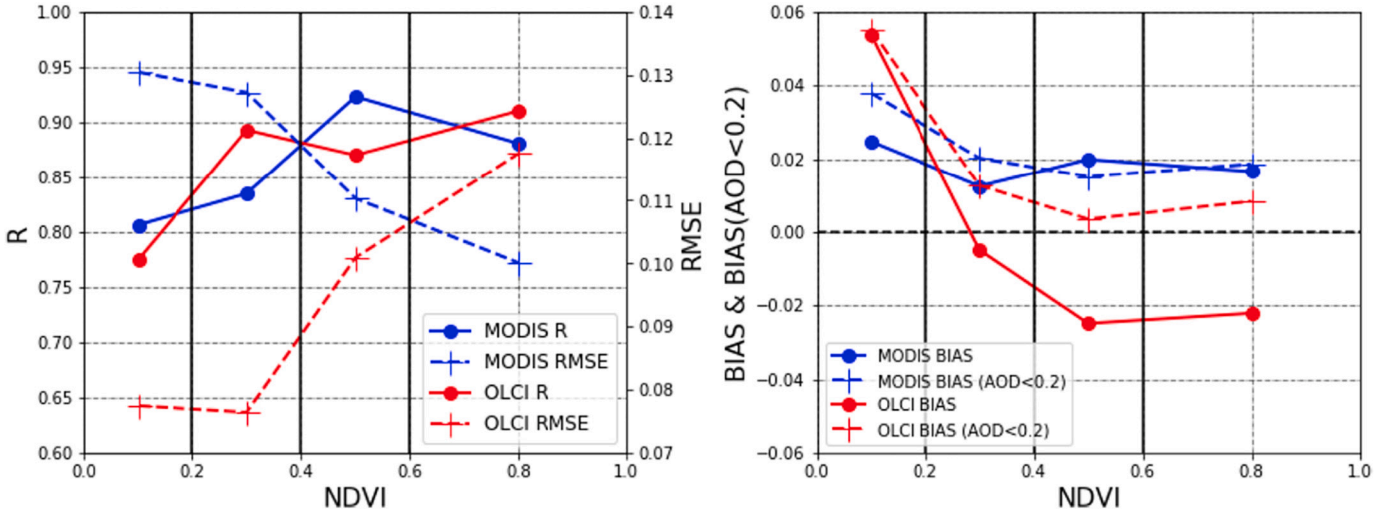

Fig. 6. Comparison of MODIS/TERRA DT + DB combined AOD and OLCI/GRASP AOD AERONET validation statistic metrics (R, RMSE, $BIAS_{TOTAL}$, $BIAS_{AOD<0.2}$) over different NDVI land surfaces.

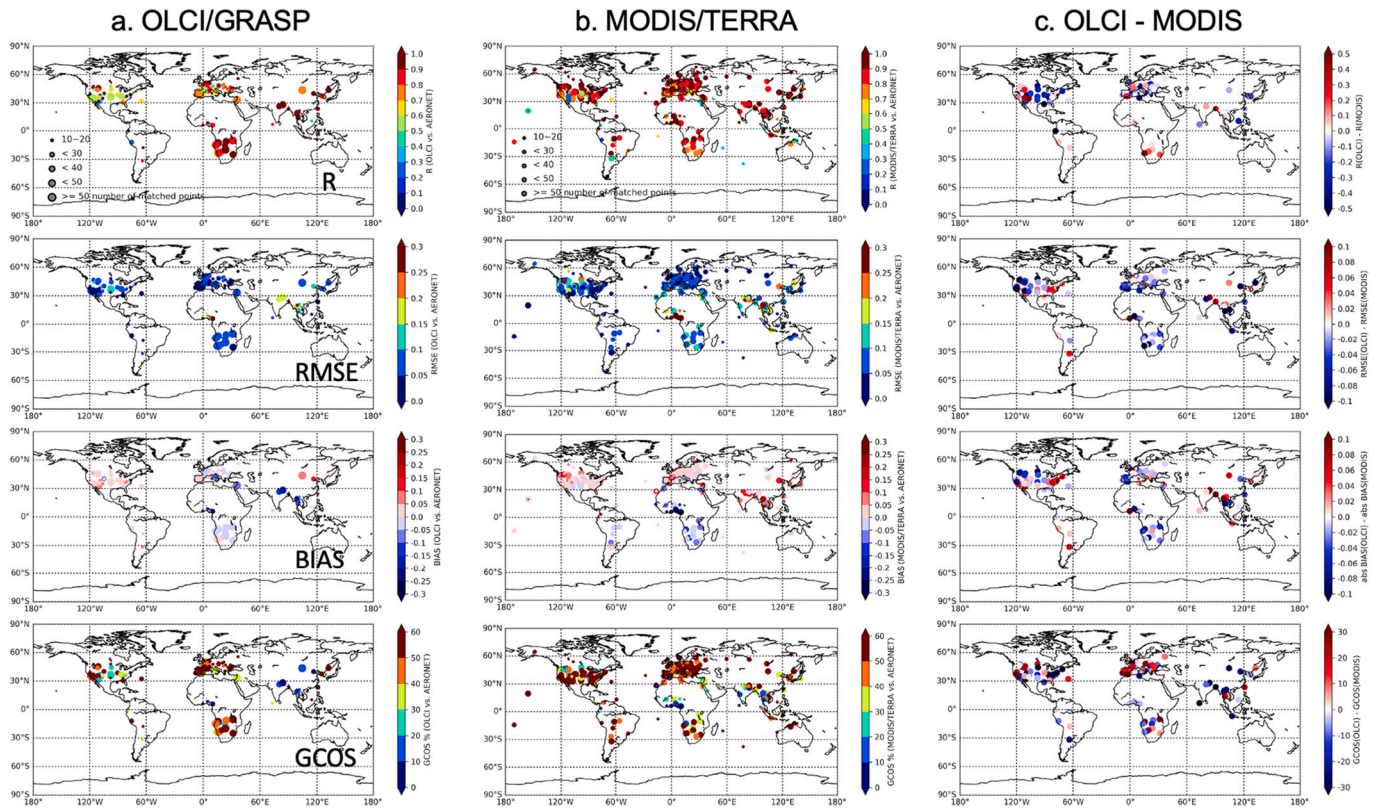

Fig. 7. Maps showing statistical metrics (R, RMSE, BIAS and GCOS) for the AOD products (a) OLCI/GRASP and (b) MODIS DT + DB. The differences (OLCI-MODIS) (c) of R, RMSE, BIAS and GCOS between OLCI and MODIS are also presented over co-covered sites.

4.3. Inter-comparison with MODIS/TERRA aerosol products

With the objective to further clarify the consistency of OLCI/GRASP and MODIS/TERRA AOD products at global scale, we analyzed the global correlation between 2 products at a spatial resolution of 0.2-degree grid box. Fig. 11a and b show the spatial distribution of monthly AOD 550 nm for August 2018 and February 2019 respectively. The differences of AOD 550 nm (OLCI/GRASP – MODIS/TERRA) averaged over a month are also presented in Fig. 11a and b. It should be noted that the depicted differences are not directly based on the monthly means, instead they are accumulated based on the daily differences that are averaged for a month. The main aerosol events can be captured by both products. For example, trans-Atlantic Canadian smoke in August 2018, Sahara dust, southern Africa biomass plume etc. Table 9 summaries the global pixel-to-pixel comparison metrics between 2 AOD 550 nm products over land and ocean separately. Over ocean, two products show rather high consistency. The correlation coefficient R is higher than 0.8, and RMSE is around 0.05, and >66% pairs are within the GCOS requirement. The OLCI/GRASP AOD is smaller than MODIS/TERRA about 0.01–0.02 over ocean. Over land, the consistency is lower than that over ocean, but it is still reasonable. The R is around 0.7 with RMSE around 0.13–0.14 and GCOS fraction around 33%. The AOD differences (OLCI – MODIS) over land vary from −0.02 (August 2018) to +0.01 (February 2019).

4.4. Inter-comparison with MODIS surface products

In addition to the comparison of aerosol products, we further compared the OLCI/GRASP land surface BRDF products with MODIS Collection 6 MCD43C1 (Schaaf and Wang, 2015), in order to identify the possible interdependencies between aerosol and surface products. Those interdependences identified can be later accounted and corrected, especially in OLCI/GRASP retrieval approach that derives aerosol and surface products simultaneously, while MODIS aerosol and surface products are generated independently. Similar to aerosol inter-comparison, we re-grid two products (MCD43C1: 0.05° and OLCI/GRASP: 10 km) into common 0.2-degree grid box.

Figs. 12 and 13 show the spatial distribution of monthly BRDF1 (a(λ)) at 560, 670 and 865 nm for August 2018 and February 2019 respectively. The differences of monthly BRDF1 (OLCI – MODIS) are also presented in Figs. 12 and 13. Table 10 summaries the global pixel-to-pixel comparison metrics between 2 surface BRDF products, including isotropic (BRDF1) parameter, volumetric (BRDF2) and geometric (BRDF3) parameters. Although mono-viewing instrument is with limited sensitivity to BRDF volumetric and geometric parameters (BRDF2 and BRDF3), the agreement between OLCI and MODIS is still reasonable that differences are <0.02 for BRDF2 and around zero for BRDF3 with RMSE <0.035 (BRDF2) and 0.015 (BRDF3). For BRDF1 isotropic term, the 2 products show very good agreement with R >0.94 and RMSE smaller than 0.035 for all 3 available common wavelengths. Globally, OLCI is around 0.01 higher than MODIS, especially over bright surface, which may be associated with the observed discrepancy between OLCI/GRASP and MODIS AOD over bright surface. Taking into account slight differences of center wavelengths and MODIS products are accumulation of 16-days TERRA and AQUA data and weighted to the day of interest, the overall global monthly mean difference of ~0.01 seems quite reasonable.

5. Discussion

5.1. Analysis of AOD discrepancy between OLCI and MODIS over India region

The pixel-to-pixel inter-comparison between MODIS Combined DT + DB and OLCI/GRASP AOD products indicated some discrepancies over India region, where the MODIS AOD is evidently higher than OLCI.

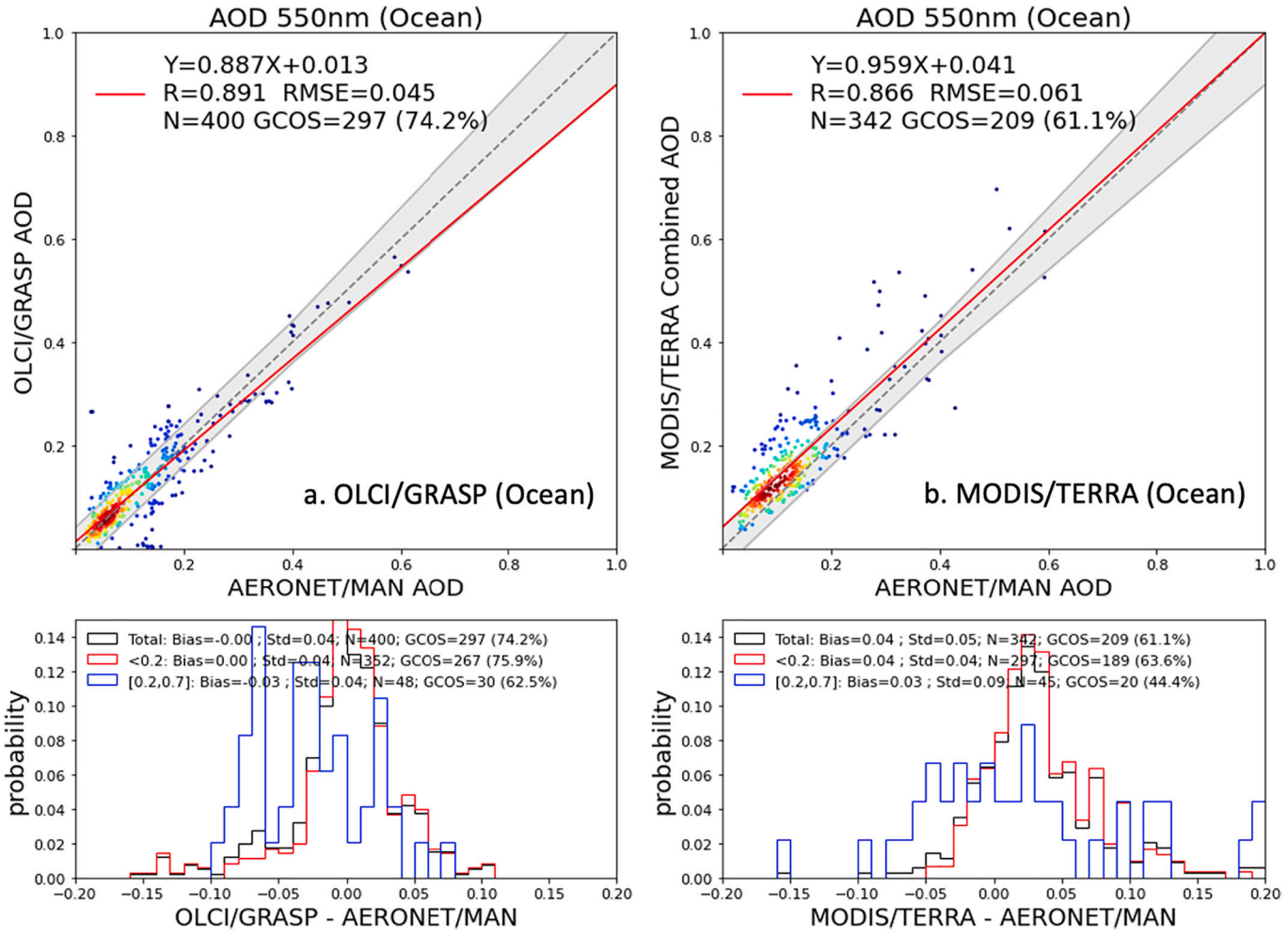

Fig. 8. Validation of (a) OLCI/GRASP and (b) MODIS/TERRA AOD 550 nm against MAN - AERONET measurements.

Fig. 14 shows the spatial distribution of OLCI (Fig. 14a) and MODIS (Fig. 14b) monthly AOD over India region for January 2019. The AOD difference (OLCI – MODIS) is presented in Fig. 14c. The two AOD products show similar spatial pattern, while the magnitude is different. For example, the high AOD over Indo-Gangetic Plain (IGP) is captured by both products, and the MODIS monthly AOD is higher than 0.9 while OLCI AOD is around 0.5–0.7.

Based on analysis of daily images and corresponding AOD products (see one case study for 2019/01/01 in Fig. 15), the potential reasons for the discrepancy can be summarized as:

a. The OLCI cloud mask (IDEPIX) probably over screens some high aerosol events; For example, Fig. 15 shows the case study of 2019/01/01. The high AOD events over AERONET site Kanpur were screened out in OLCI data as cloud.
b. The difference of OLCI and MODIS/TERRA orbits may result in the discrepancy of monthly OLCI and MODIS AOD. Fig. 15 also shows the difference in the orbit coverage, and this difference varies day by day.
c. The opposite signs of bias for MODIS and OLCI AOD products may also be another factor contribute to the AOD discrepancy. We compared one-year AERONET validation over Kanpur (the geo-location of AERONET site Kanpur is labeled as cross in Fig. 15b), and the results are shown in Fig. 16. Both of MODIS and OLCI AOD products show good correlation with AERONET ($R > 0.8$), however, MODIS has a positive bias ~ +0.14, while OLCI has a negative bias ~ –0.15.

5.2. *Evaluation of OLCI/GRASP diagnosed detailed aerosol properties (AE and SSA)*

One of the advantages of the GRASP algorithm is that it searches solution in continuous space without using location specific a priori aerosol models. GRASP/Models approach adapted for OLCI processing assuming aerosol as an external mixture of 4 aerosol components (Lopatin et al., 2021) that, in principle, limits the degree of freedom of the retrieval to some extent in comparison with GRASP/Optimized or GRASP/HP (High Precision) approaches, even though the aerosol components can be freely mixed with no constraints (Chen et al., 2020). As a result of utilization GRASP/Models approach, we still were able to diagnose detailed aerosol properties (e.g. AE and spectral SSA) from OLCI/GRASP retrievals. Despite the single viewing instrument may not be sufficiently sensitive to these parameters related with aerosol size and absorption, we evaluate OLCI/GRASP AE (440/870) and spectral SSA (440, 550, 670, 865 and 1020 nm) against AERONET products.

In AE validation analysis, we followed the similar strategy as Chen et al. (2020) that further requiring the satellite retrieved AOD (550 nm) >0.2 to ensure the AE quality. Fig. 17 shows the global validation of OLCI/GRASP AE (440/870) against AERONET over land (Fig. 17a) and ocean (Fig. 17b). OLCI/GRASP AE over ocean ($R = 0.751$, RMSE = 0.386) is more reliable than that over land ($R = 0.526$, RMSE = 0.531). Generally, over land, when fine mode dominant (AE > 1.0), OLCI/GRASP tends to underestimate AE, while over ocean, when coarse mode dominant (AE < 1.0), OLCI/GRASP tends to overestimates AE. In addition, the retrieval of AE over bright surface seems problematic at the

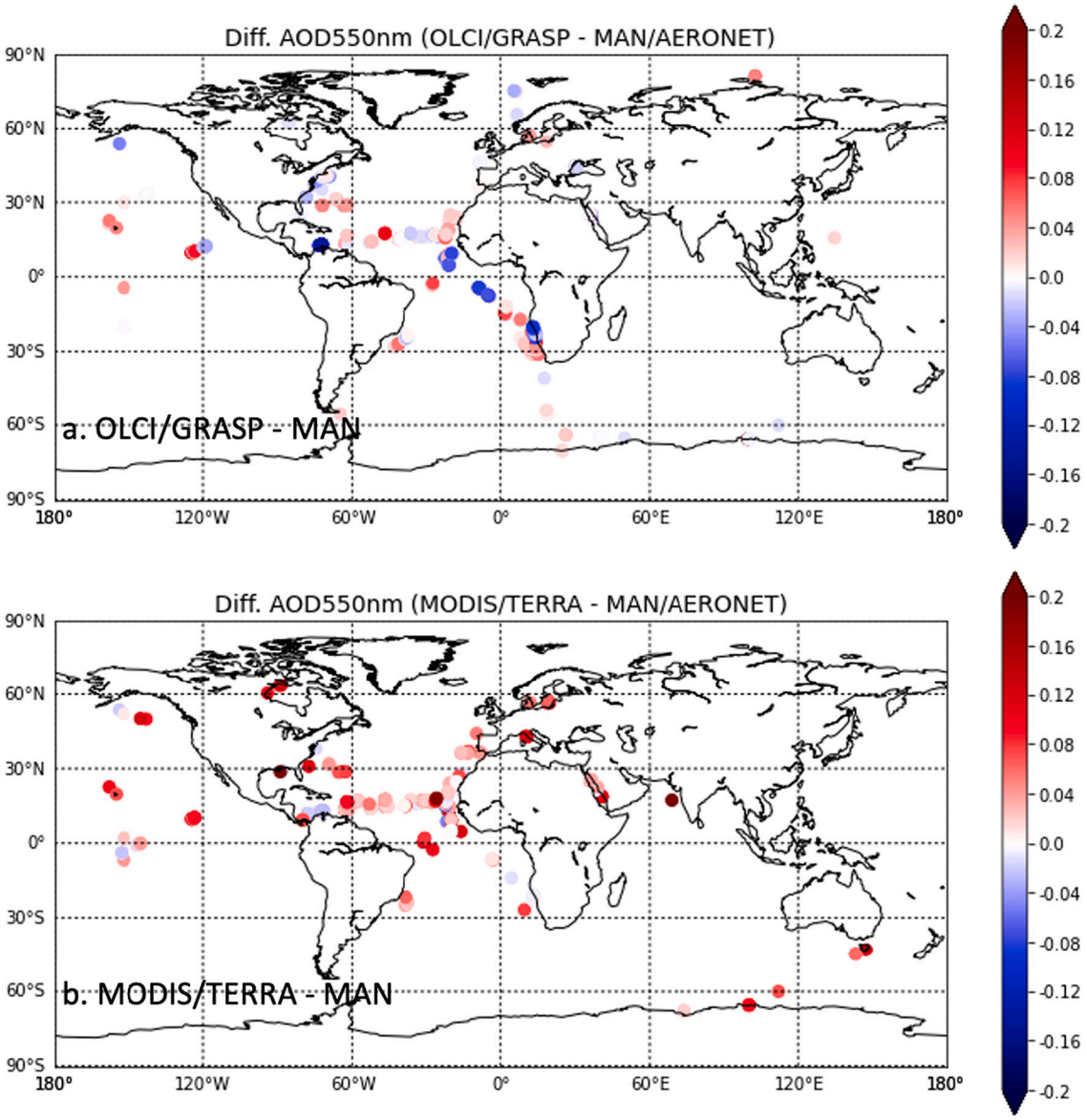

Fig. 9. Spatial distribution of differences of AOD 550 nm between MODIS/TERRA, OLCI/GRASP and MAN/AERONET.

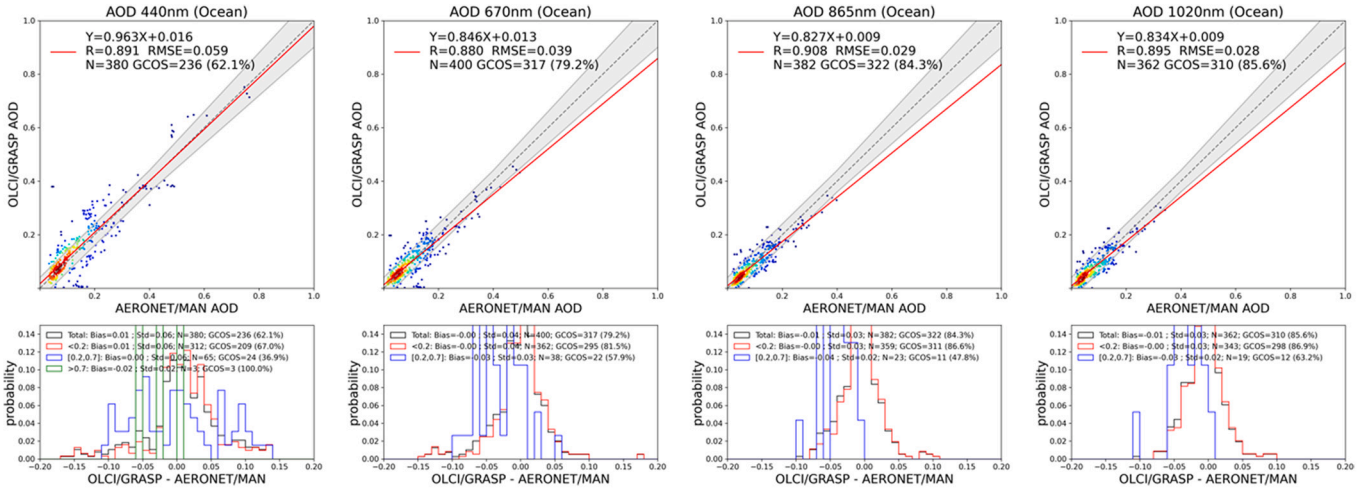

Fig. 10. Validation of OLCI/GRASP spectral AOD at 440, 670, 865 and 1020 nm against MAN/AERONET measurements.

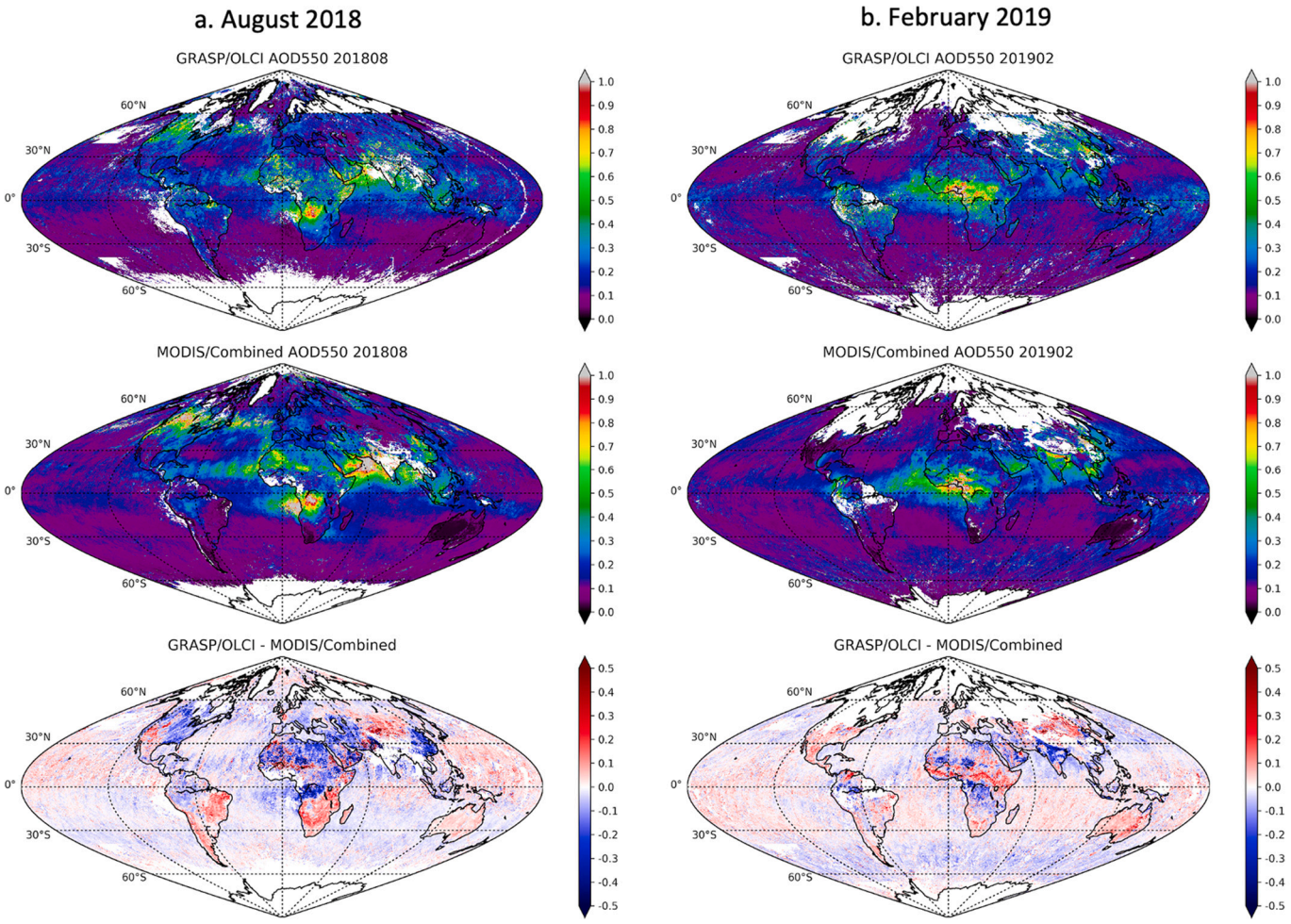

Fig. 11. Spatial distribution of monthly (a. August 2018; b. February 2019) AOD 550 nm from OLCI/GRASP and MODIS/TERRA DT + DB combined products. The difference of AOD 550 nm averaged over a month is presented as OLCI/GRASP – MODIS/TERRA combined DT + DB.

Table 9
Summary of global pixel-to-pixel comparison metrics between OLCI/GRASP and MODIS/TERRA DT + DB combined AOD at 550 nm for 2 months (August 2018 and February 2019).

YYYY/MM	Land/Ocean (Num. of pairs)	R	RMSE	GCOS (%)	Diff. AOD OLCI– MODIS
2018/08	Land (822730)	0.717	0.141	33.7	−0.02
	Ocean (1184333)	0.877	0.054	66.6	−0.02
2019/02	Land (487162)	0.734	0.129	33.8	0.01
	Ocean (1028456)	0.848	0.053	66.0	−0.01

current stage, which is possibly due to the lack of sensitivity and may be associated with overestimation of AOD and surface albedo there. These results provide some general ideas and valuable basis for considering possible improvement of the representative aerosol models in GRASP/Models approach.

Aerosol absorption is a key information to pin down aerosol climate effect evaluation (Samset et al., 2018; Stier et al., 2007; Chen et al., 2019; Mallet et al., 2021), while it is typically difficult or even impossible to obtain using single viewing radiometer because of low sensitivity. Nonetheless, since we adopted a priori information for angular properties of surface reflectance in retrieval and therefore additionally constrained the solution, we conducted quantitively evaluation of the derived OLCI/GRASP spectral SSA results against AERONET L2 inversion products (Dubovik and King, 2000). Because the sensitivity study indicates the improvement in accuracy of retrieved SSA with the increase of AOD (Dubovik et al., 2000; Sinyuk et al., 2020), AERONET L2 SSA products were provided for moderate and high aerosol abundance (AOD 440 nm $\geq$0.4). Also, Chen et al. (2020) showed that the agreement between satellite and AERONET SSA clearly improves with the increase of AOD levels. In this regard, since retrieval of SSA is not expected from single view instruments, we select the OLCI/GRASP data for the validation of SSA with even higher limit of AOD 550 nm $\geq$0.5. In addition, the time window between OLCI overpass and AERONET retrievals extend to ±180 mins. Fig. 18 shows the validation of OLCI/-GRASP spectral SSA against AERONET SSA at 440, 550, 670, 865 and 1020 nm. Note the statistic is based on moderate and high aerosol abundance (AERONET AOD 440 nm $\geq$0.4 and OLCI/GRASP AOD 550 nm $\geq$0.5), and therefore the most of cases are over land. To compare with the recent study by Schutgens et al. (2021) of evaluation of satellite SSA products, OLCI/GRASP SSA validation metrics for these highly selected data are somewhat comparable with those from MAP instrument and instrument with ultraviolet measurements. For example, the BIAS at 550 nm is around −0.01 and RMSE is 0.026. At the same time, it is clear that detailed products such as AE and SSA are of rather limited accuracy, and it may also be associated with the limited information content in single-view observation geometry (Fougnie et al., 2020) that need to further evaluation with future efforts.

6. Summary and conclusion

In this study, we have described retrieval of aerosol and surface

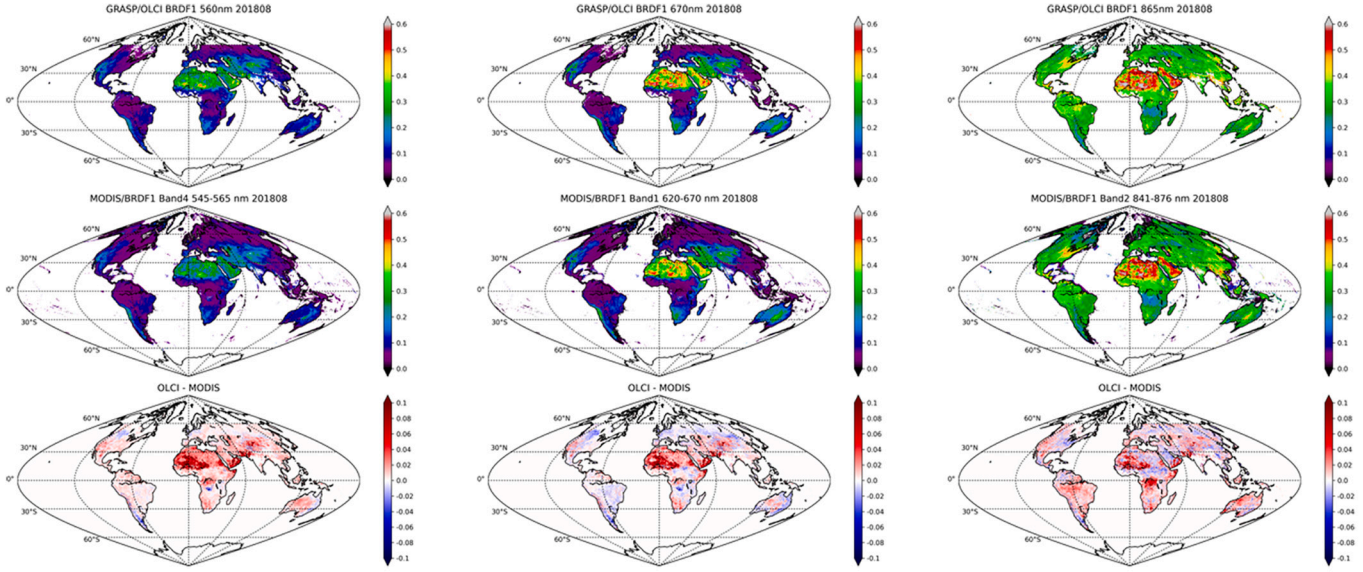

Fig. 12. Spatial distribution of monthly (August 2018) BRDF1 (isotropic parameter) from OLCI/GRASP and MODIS MCD43C1 at 560, 670 and 865 nm.

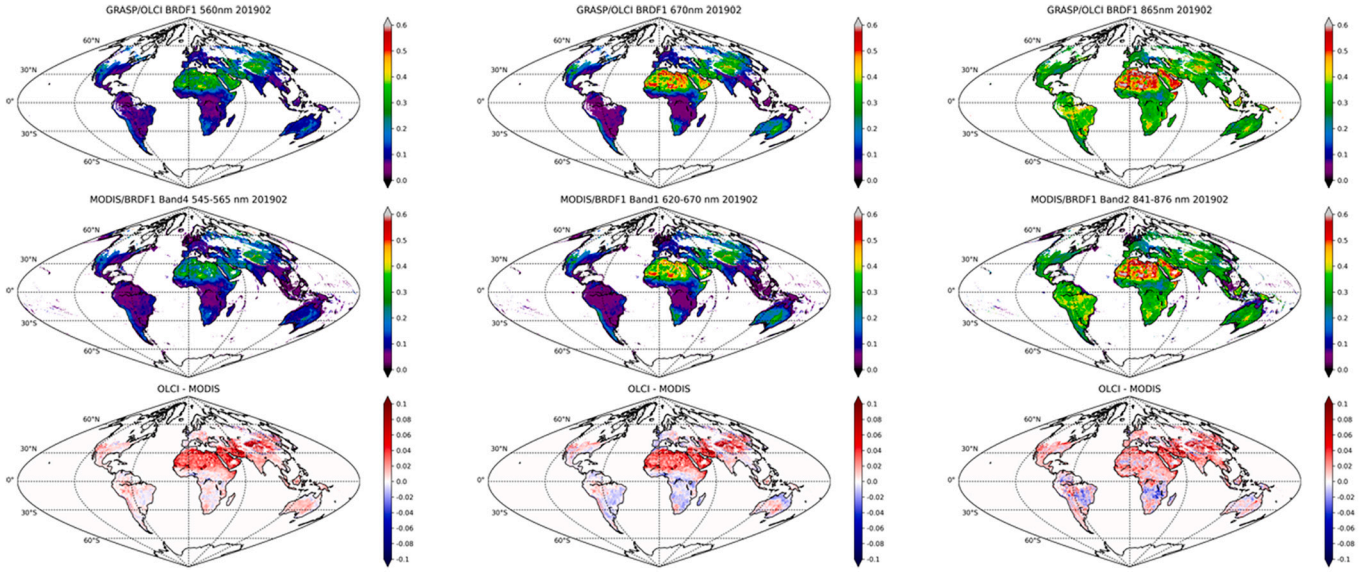

Fig. 13. The same as Fig. 12, but for February 2019.

Table 10
Summary of global pixel-to-pixel comparison metrics between OLCI/GRASP and MODIS MCD43C1 BRDF at 560, 670 and 865 nm for 2 months (August 2018 and February 2019).

YYYY/MM	BRDF parameters	R	RMSE	Diff. BRDF OLCI– MODIS
2018/08	BRDF1 iso 560 nm	0.948	0.031	0.01
	BRDF1 iso 670 nm	0.978	0.030	0.01
	BRDF1 iso 865 nm	0.946	0.030	0.01
	BRDF2 vol	0.768	0.035	0.02
	BRDF3 geo	0.865	0.008	0.00
2019/02	BRDF1 iso 560 nm	0.955	0.030	0.01
	BRDF1 iso 670 nm	0.980	0.031	0.01
	BRDF1 iso 865 nm	0.944	0.033	0.01
	BRDF2 vol	0.611	0.034	0.01
	BRDF3 geo	0.829	0.012	0.00

products from OLCI/Sentinel-3A based on the GRASP algorithm. The initial results generated the baseline processing based on retrieval configuration adopted from the former MERIS/GRASP processing (e.g. see Dubovik et al., 2021b) that showed reasonable AOD product but revealed several issues such as the non-negligible bias for lower AOD. Therefore, we performed a series of retrieval tests over land and ocean to address the observed issues in that baseline approach. The positive evolution of OLCI/GRASP aerosol retrieval was evidently observed by using a priori constraints on land and ocean surface BRDF, optimization of OLCI spectral information, using rather general a priori constraints on retrieved aerosol parameters, optimization of RT calculations, etc. The key findings of the OLCI/GRASP land and ocean aerosol retrieval tests can be summarized as:

- Over ocean the following useful retrieval adjustments were identified:

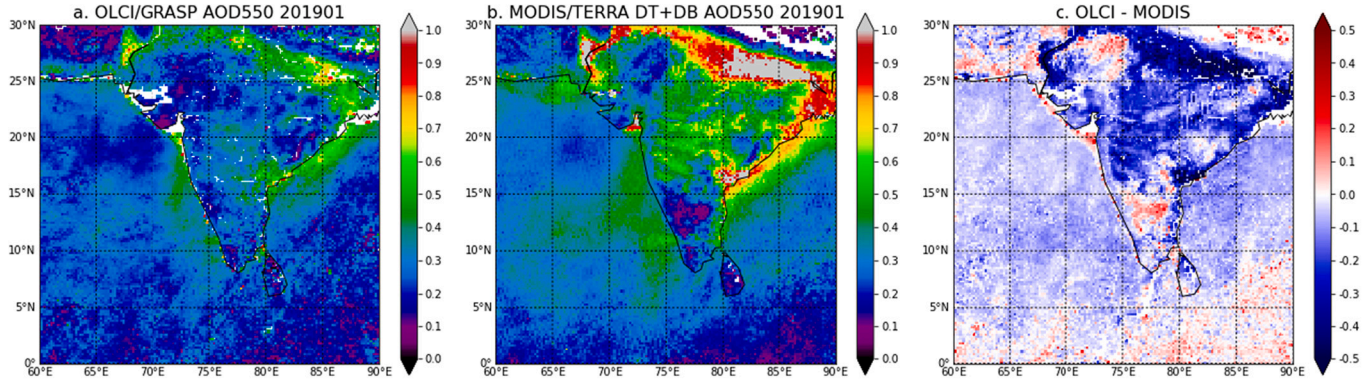

Fig. 14. Spatial distribution of monthly (January 2019) AOD 550 nm from (a) OLCI/GRASP and (b) MODIS/TERRA DT + DB combined products over India region. The difference of AOD 550 nm averaged over a month is also presented as (c) OLCI - MODIS.

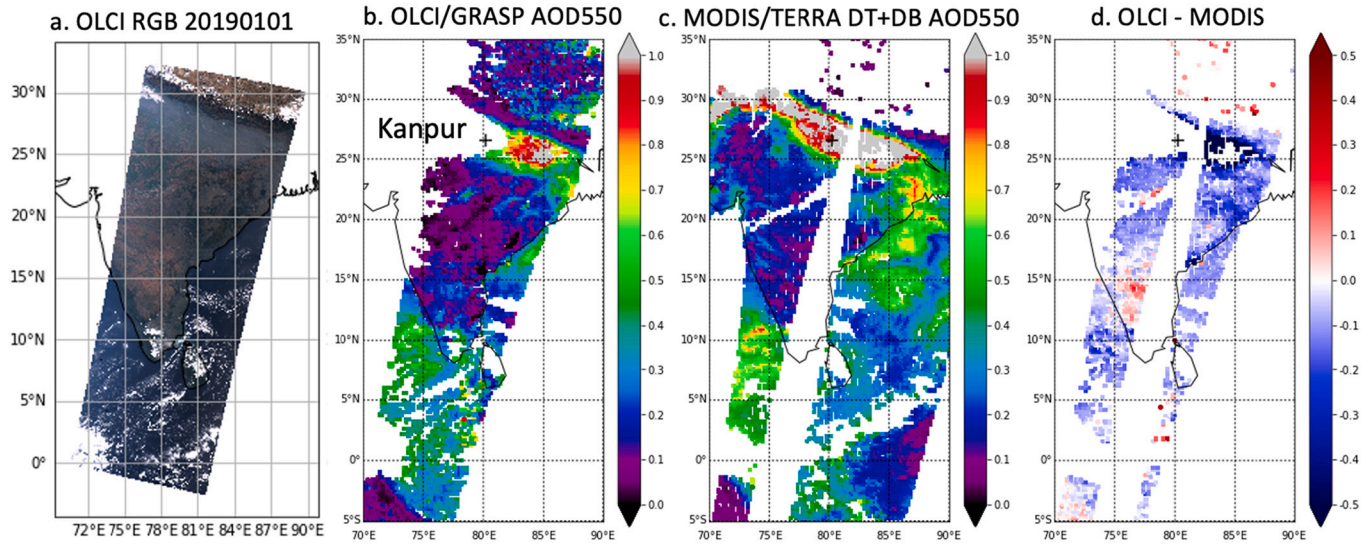

Fig. 15. The case study of AOD events of 2019/01/01 over India region, from left to right: (a) OLCI RGB, (b) OLCI/GRASP AOD 550 nm, (c) MODIS/TERRA DT + DB AOD 550 nm, and (d) OLCI-MODIS AOD.

- the constraining angular ocean surface BRDF properties (δ_{Fr} and σ^2) using known values of wind speed improved the OLCI/GRASP AOD retrieval significantly;
- The use of OLCI near infrared 1020 nm measurements showed some improvements as was expected over the ocean, the surface at 1020 nm is nearly black and mostly affected by coarse mode dominant aerosol;
- the application of low weights / high uncertainty to blue channels (412.5, 442.5, and 490 nm), in which the ocean surface signal is radiometrically complex leading to a very high complexity for accurate reflectance modeling, proved to be useful for further improvement of the OLCI/GRASP ocean AOD retrieval.

• Over land, the following useful retrieval adjustments were identified:

- the use of a surface climatology (POLDER-3/GRASP in this context) for constraining three Ross-Li BRDF parameters as follows: (i) initial guess for isotropic term $a_{iso}(\lambda)$, and (ii) a priori estimates for volumetric and geometric terms (a_{vol} and a_{geom}) that drive the angular properties of BRDF. It should be also noted though that the identified improvements were less significant than the use of a priori constants for ocean surface reflectance;
- the assumption of spectral independence of BRDF volumetric and geometric terms (a_{vol} and a_{geom}) helped to reduce the number of unknowns and overall improved the retrieval;
- the use of stronger constraints on spatial and temporal (though much weaker than for spatial distribution) variability of aerosol composition;
- the use of a vector radiative transfer model in the forward modeling calculation is observed to be helpful for reducing the bias for low AOD conditions.

The algorithm tuned in conducted ocean and land tests, was used to process one-year (June 2018 to May 2019) OLCI/Sentinel-3A data. The results are validated globally against AERONET all available measurements, as well as MAN ship-borne deep ocean measurements. The validation results are also compared with MODIS/TERRA DT + DB combined AOD products. The intercomparisons of global OLCI/GRASP and MODIS pixel-to-pixel aerosol and surface products are also performed. The findings can be summarized as follows:

a. Over ocean, OLCI/GRASP AOD shows similar validation metrics with MODIS/TERRA against AERONET ocean sites with a bit lower correlation coefficient but higher GCOS and smaller biases. OLCI/GRASP AOD validation against MAN measurements shows nearly zero biases over deep ocean, while MODIS/TERRA has known positive biases around 0.03–0.04. The global pixel-to-pixel comparison between 2 AOD products also indicates very high consistency over

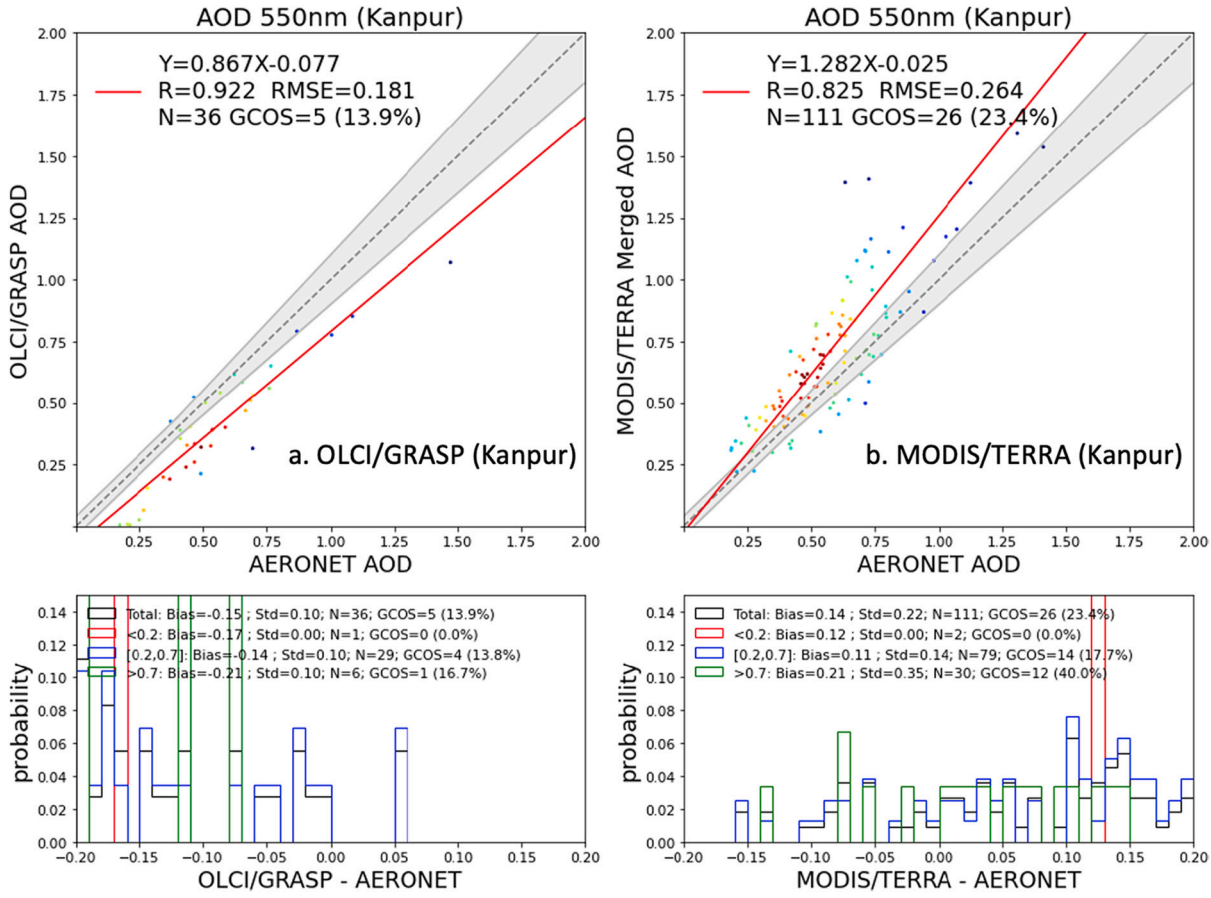

Fig. 16. Validation of (a) OLCI/GRASP AOD and (b) MODIS/TERRA DT + DB AOD 550 nm against AERONET over Kanpur (26.513°N, 80.232°E).

ocean based on millions of pairs, with correlation coefficient higher than 0.84, RMSE around 0.05, differences within ~0.02 (MODIS/TERRA higher than OLCI).

b. Over land, OLCI/GRASP shows similar performance against AERONET as MODIS DT + DB combined product with $R > 0.87$, GCOS>45%, BIAS<0.02. Over bright surface (NDVI<0.2), 2 products are all less accurate than over other surfaces, and MODIS/TERRA is more accurate than OLCI/GRASP. For mixture of bare soil and vegetated surfaces ($0.2 \leq$ NDVI<0.4), OLCI/GRASP seems to provide more accurate results than MODIS/TERRA. For vegetated surface (NDVI≥0.4), the two products show overall similar statistics. Even though both OLCI/GRASP and MODIS/TERRA products show good agreement with AERONET, the differences between 2 products are higher than that over ocean. The OLCI and MODIS pixel-to-pixel inter-comparison indicates a correlation coefficient around 0.7 and 33% pairs satisfy the GCOS requirement, in contrast with $R > 0.84$ GCOS>66% over ocean. For example, over India, the AOD differences are high between OLCI and MODIS. According to AERONET sites validation over India, this is partially due to the opposite signs of bias for 2 products, e.g., MODIS/TERRA over Kanpur ($R = 0.83$, BIAS = +0.14); OLCI/GRASP over Kanpur ($R = 0.92$, BIAS = –0.15). In addition, the cloud mask and the different orbits may also result in the AOD discrepancy.

c. The analysis of detailed aerosol properties (AE and spectral SSA) derived from OLCI/GRASP shows reasonable agreement with AERONET products. Generally, the OLCI/GRASP AE over ocean is with higher quality than that over land. Both over land and ocean, the overestimation of AE when coarse mode dominant is present. While, the current AE over bright surface seems problematic due to the lack of sensitivity to particle size especially for low aerosol conditions. The preliminary validation of OLCI/GRASP spectral SSA against AERONET for rather strictly selected cased (with moderate and high aerosol loading events with OLCI AOD 550 nm $\geq$ 0.5) shows encouraging agreement, for example, BIAS within 0.01 and RMSE within 0.03 for SSA at 550 nm, that is comparable with SSA products from MAP measurements. Therefore, the OLCI/GRASP products for diagnosed detailed aerosol properties are of interest for further considerations.

d. The intercomparison between OLCI/GRASP monthly BRDF product with MODIS product shows good consistency, for example, the differences for isotropic term are within 0.01 and RMSE around 0.03. The main discrepancy is seen over the bright surface, where OLCI/GRASP tends to report higher surface reflectance.

Thus, based on the results of conducted study, it is possible to conclude that the developed OLCI-A/GRASP retrieval and tested on one year time-series observations is appropriate for systematic processing of OLCI observations and producing of aerosol and surface retrieval product of quality comparable to the community reference MODIS product. Moreover, it can be noted, that MODIS aerosol and surface products are generated by several independent teams and algorithms (AOD/DT ocean, AOD/DT land, AOD/DB land, surface BRDF) and relies on a number of locally or regionally specific assumptions and constraints. In these regards, OLCI/GRASP algorithm generates both aerosol and surface products simultaneously and in a fully consistent manner both over land and ocean. In addition, for aerosol properties the OLCI/GRASP retrieval uses exactly the same aerosol model, initial guesses and a priori constraints globally (though a slightly different over land and ocean).

Finally, some remaining issues in OLCI/GRASP retrieval should be

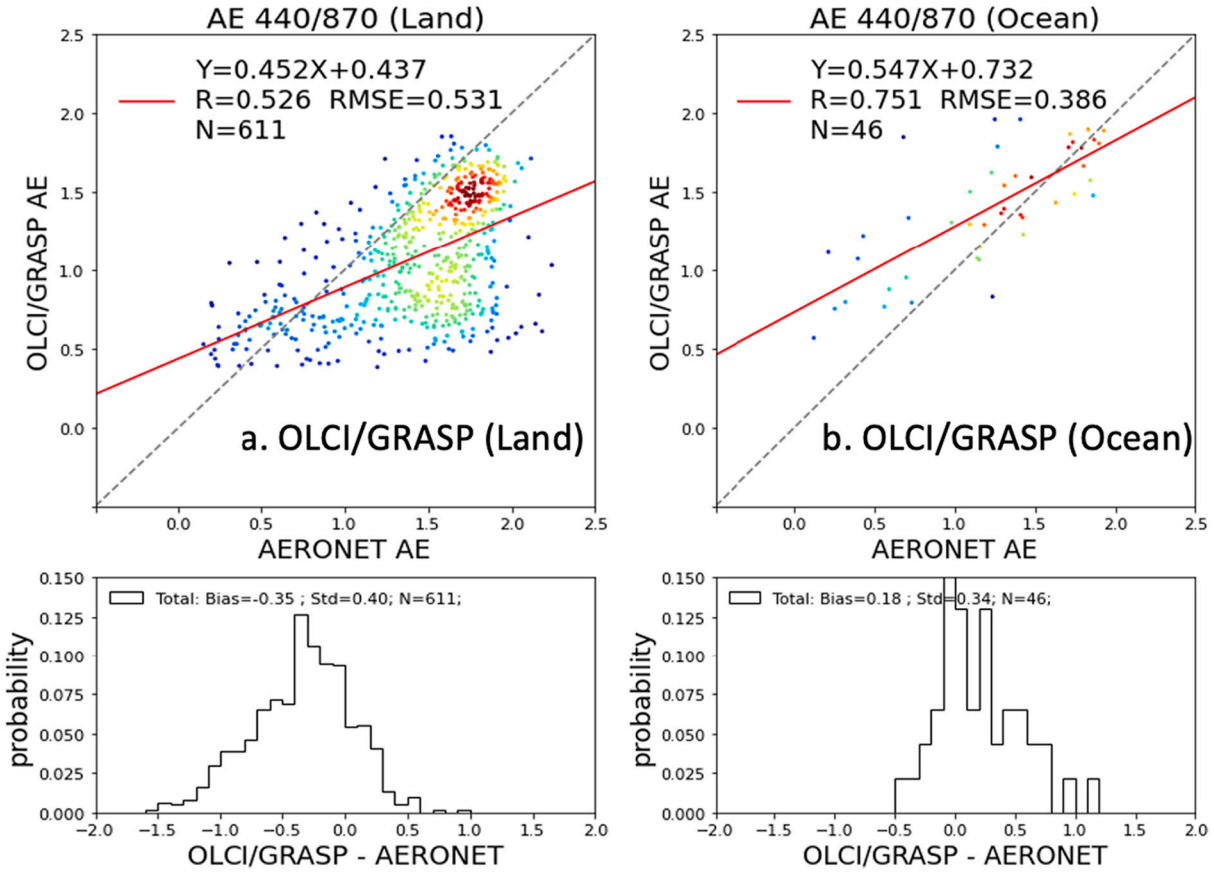

Fig. 17. Validation of OLCI/GRASP AE (440/870) against AERONET over (a) land and (b) ocean.

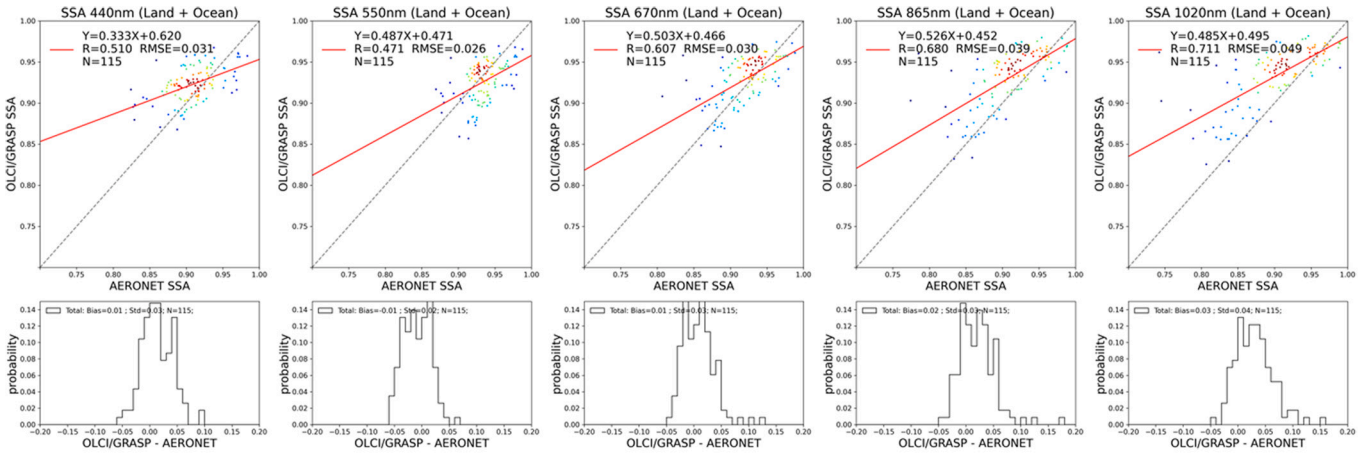

Fig. 18. Validation of OLCI/GRASP spectral SSA at 440, 550, 670, 865 and 1020 nm against AERONET L2 inversion products.

acknowledged too. Specifically, the following aspects OLCI/GRASP processing need to be improved in future efforts: (i) current study didn't consider any optimization of used cloud mask that certainly limited accuracy of OLCI/GRASP, the appropriate efforts need to be done in future; (ii) the described OLCI/GRASP retrieval realized on historical POLDER-3 surface climatology, this climatology can be certainly updated and improved; (iii) further adjustments in the selection of predefined aerosol models can be done to refine and tune GRASP retrieval approach for information content of OLCI observations; (iv) additional improvements, such as considering windspeed direction, in ocean surface reflectance are planned to introduce in the future efforts; (v) present study didn't specifically consider aerosol retrieval over ice, snow and coastal water, these challenging situations are part of future plans of OLCI/GRASP retrieval evolution.

Data availability

The OLCI/GRASP Version 1 aerosol and surface products are publicly available at GRASP-OPEN website (http://www.grasp-open.com/products/olci-data-release/).

Author contributions

The GRASP team (OD, PL, DF, AL, TL, CC, CM, YK) developed the methodology for Sentinel-3A/OLCI. CC, OD, PL, AH, DF and CM carried out the retrieval tests. The results were widely exchanged and discussed with the EUMETSAT team (JC, BD, TM, BB). JF and RP helped the Sentinel-3A/OLC L1B gas correction. The Cloudflight team (AH, LB, DM, MA) prepared the input data and carried out the processing. CC and OD wrote the manuscript with contributions from all coauthors.

Declaration of Competing Interest

The authors declare that they have no known competing financial interests or personal relationships that could have appeared to influence the work reported in this paper.

Acknowledgements

The authors would like to gratefully acknowledge EUMETSAT for continuous support of OLCI/GRASP development within framework of the project: Risk mitigation study for Aerosol Optical Depth product retrieval from Sentinel-3 OLCI through the contract EUM/CO/19/4600002258/JCh. We would like to thank the AERONET, AERONET/MAN networks and MODIS mission and aerosol science team for production the data and making their data available for the community. All PIs and their staff of AERONET stations and AERONET/MAN for maintaining the instrument are gratefully acknowledged.

References

Benavent-Oltra, J.A., Román, R., Granados-Muñoz, M.J., Pérez-Ramírez, D., Ortiz-Amezcua, P., Denjean, C., Lopatin, A., Lyamani, H., Torres, B., Guerrero-Rascado, J. L., Fuertes, D., Dubovik, O., Chaikovsky, A., Olmo, F.J., Mallet, M., Alados-Arboledas, L., 2017. Comparative assessment of GRASP algorithm for a dust event over Granada (Spain) during ChArMEx-ADRIMED 2013 campaign. Atmos. Meas. Tech. 10 (11), 4439–4457. https://doi.org/10.5194/amt-10-4439-2017.

Benavent-Oltra, J.A., Román, R., Casquero-Vera, J.A., Pérez-Ramírez, D., Lyamani, H., Ortiz-Amezcua, P., Bedoya-Velásquez, A.E., de Arruda Moreira, G., Barreto, Á., Lopatin, A., Fuertes, D., Herrera, M., Torres, B., Dubovik, O., Guerrero-Rascado, J.L., Goloub, P., Olmo-Reyes, F.J., Alados-Arboledas, L., 2019. Different strategies to retrieve aerosol properties at night-time with the GRASP algorithm. Atmos. Chem. Phys. 19 (22), 14149–14171. https://doi.org/10.5194/acp-19-14149-2019.

Boucher, O., Randall, D., Artaxo, P., Bretherton, C., Feingold, G., Forster, P., Kerminen, V., Kondo, Y., Liao, H., Lohmann, U., Rasch, P., Satheesh, S., Sherwood, S., Stevens, B., Zhang, X., Qin, D., Plattner, G., Tignor, M., Allen, S., Boschung, J., Nauels, A., Xia, Y., Bex, V., Midgley, P., 2013. In: Stocker, T.F., Qin, D., Plattner, G.-K., Tignor, M., Allen, S.K., Boschung, J., Nauels, A., Xia, Y. (Eds.), Clouds and Aerosols, in Climate Change 2013: The Physical Science Basis. Contribution of Working Group I to the Fifth Assessment Report of the Intergovernmental Panel on Climate Change. Cambridge University Press, Cambridge, United Kindom and New York, NY, USA [online] Available from. http://www.ipcc.ch/pdf/assessment-report/ar5/wg1/WG1AR5_Chapter07_FINAL.pdf.

Chen, C., Dubovik, O., Henze, D.K., Chin, M., Lapyonok, T., Schuster, G.L., Ducos, F., Fuertes, D., Litvinov, P., Li, L., Lopatin, A., Hu, Q., Torres, B., 2019. Constraining global aerosol emissions using POLDER/PARASOL satellite remote sensing observations. Atmos. Chem. Phys. 19 (23), 14585–14606. https://doi.org/10.5194/acp-19-14585-2019.

Chen, C., Dubovik, O., Fuertes, D., Litvinov, P., Lapyonok, T., Lopatin, A., Ducos, F., Derimian, Y., Herman, M., Tanré, D., Remer, L., Lyapustin, A., Sayer, A., Levy, R., Hsu, N.C., Descloitres, J., Li, L., Torres, B., Karol, Y., Herrera, M., Herreras, M., Aspetsberger, M., Wanzenboeck, M., Bindreiter, L., Marth, D., Hangler, A., Federspiel, C., 2020. Validation of GRASP algorithm product from POLDER/PARASOL data and assessment of multi-angular polarimetry potential for aerosol monitoring. Earth Syst. Sci. Data 12 (4), 3573–3620. https://doi.org/10.5194/essd-12-3573-2020.

Chin, M., Kahn, R.A., Remer, L.A., Yu, H., Rind, D., Feingold, G., Quinn, P.K., Schwartz, S.E., Streets, D.G., DeCola, P., 2009. Atmospheric Aerosol Properties and Climate Impacts. Diane Publishing.

Cox, C., Munk, W., 1954. Measurement of the roughness of the sea surface from photographs of the sun's glitter. J. Opt. Soc. Am. 44 (11), 838. https://doi.org/10.1364/josa.44.000838.

Donlon, C., Berruti, B., Buongiorno, A., Ferreira, M.H., Féménias, P., Frerick, J., Goryl, P., Klein, U., Laur, H., Mavrocordatos, C., Nieke, J., Rebhan, H., Seitz, B., Stroede, J., Sciarra, R., 2012. The global monitoring for environment and security (GMES) Sentinel-3 mission. Remote Sens. Environ. 120, 37–57. https://doi.org/10.1016/j.rse.2011.07.024.

Doppler, L., Preusker, R., Bennartz, R., Fischer, J., 2014. K-bin and k-IR: K-distribution methods without correlation approximation for non-fixed instrument response function and extension to the thermal infrared-applications to satellite remote sensing. J. Quant. Spectrosc. Radiat. Transf. 133, 382–395. https://doi.org/10.1016/j.jqsrt.2013.09.001.

Dubovik, O., King, M.D., 2000. A flexible inversion algorithm for retrieval of aerosol optical properties from sun and sky radiance measurements. J. Geophys. Res. Atmos. 105 (D16), 20673–20696. https://doi.org/10.1029/2000JD900282.

Dubovik, O., Smirnov, A., Holben, B.N., King, M.D., Kaufman, Y.J., Eck, T.F., Slutsker, I., 2000. Accuracy assessments of aerosol optical properties retrieved from aerosol robotic network (AERONET) sun and sky radiance measurements. J. Geophys. Res. Atmos. 105 (D8), 9791–9806. https://doi.org/10.1029/2000JD900040.

Dubovik, O., Herman, M., Holdak, A., Lapyonok, T., Tanré, D., Deuzé, J.L., Ducos, F., Sinyuk, A., Lopatin, A., 2011. Statistically optimized inversion algorithm for enhanced retrieval of aerosol properties from spectral multi-angle polarimetric satellite observations. Atmos. Meas. Tech. 4 (5), 975–1018. https://doi.org/10.5194/amt-4-975-2011.

Dubovik, O., Lapyonok, T., Litvinov, P., Herman, M., Fuertes, D., Ducos, F., Torres, B., Derimian, Y., Huang, X., Lopatin, A., Chaikovsky, A., Aspetsberger, M., Federspiel, C., 2014. GRASP: a versatile algorithm for characterizing the atmosphere. SPIE Newsroom. https://doi.org/10.1117/2.1201408.005558.

Dubovik, O., Schuster, G.L., Xu, F., Hu, Y., Bösch, H., Landgraf, J., Li, Z., 2021a. Grand challenges in satellite remote sensing. Front. Remote Sens. 2, 619818 https://doi.org/10.3389/frsen.2020.603650.

Dubovik, O., Fuertes, D., Lytvynov, P., Lopatin, A., Lapyonok, T., Doubovik, I., Xu, F., Ducos, F., Chen, C., Torres, B., Derimian, Y., Li, L., Herrera, M., Karol, Y., Matar, C., Schuster, G., Espinosa, R., Puthukkudy, A., Li, Z., Juergen, F., Preusker, R., Cuesta, J., Kreuter, A., Cede, A., Aspetsberger, M., Marth, D., Bindreiter, L., Hangler, A., Lanzinger, V., Holter, C., Federspiel, C., 2021b. A comprehensive description of multi-term LSM for applying multiple a priori constraints in problems of atmospheric remote sensing: GRASP algorithm, concept, and applications. Front. Remote Sens. https://doi.org/10.3389/frsen.2021.706851.

Espinosa, W.R., Remer, L.A., Dubovik, O., Ziemba, L., Beyersdorf, A., Orozco, D., Schuster, G., Lapyonok, T., Fuertes, D., Martins, J.V., 2017. Retrievals of aerosol optical and microphysical properties from imaging polar nephelometer scattering measurements. Atmos. Meas. Tech. 10 (3), 811–824. https://doi.org/10.5194/amt-10-811-2017.

Espinosa, W.R., Martins, J.V., Remer, L.A., Dubovik, O., Lapyonok, T., Fuertes, D., Puthukkudy, A., Orozco, D., Ziemba, L., Thornhill, K.L., Levy, R., 2019. Retrievals of aerosol size distribution, spherical fraction, and complex refractive index from airborne in situ angular light scattering and absorption measurements. J. Geophys. Res. Atmos. 124 (14), 7997–8024. https://doi.org/10.1029/2018JD030009.

Fougnie, B., Chimot, J., Vázquez-Navarro, M., Marbach, T., Bojkov, B., 2020. Aerosol retrieval from space – how does geometry of acquisition impact our ability to characterize aerosol properties. J. Quant. Spectrosc. Radiat. Transf. 256, 107304 https://doi.org/10.1016/j.jqsrt.2020.107304.

Frouin, R., Pelletier, B., 2015. Bayesian methodology for inverting satellite ocean-color data. Remote Sens. Environ. 159, 332–360. https://doi.org/10.1016/j.rse.2014.12.001.

Frouin, R., Schwindling, M., Deschamps, P.-Y., 1996. Spectral reflectance of sea foam in the visible and near infrared: in-situ measurements and remote sensing implications. J. Geophys. Res. Oceans 101, 14361–14371. https://doi.org/10.1029/96JC00629.

Giles, D.M., Sinyuk, A., Sorokin, M.G., Schafer, J.S., Smirnov, A., Slutsker, I., Eck, T.F., Holben, B.N., Lewis, J.R., Campbell, J.R., Welton, E.J., Korkin, S.V., Lyapustin, A.I., 2019. Advancements in the aerosol robotic network (AERONET) version 3 database – automated near-real-time quality control algorithm with improved cloud screening for sun photometer aerosol optical depth (AOD) measurements. Atmos. Meas. Tech. 12 (1), 169–209. https://doi.org/10.5194/amt-12-169-2019.

Holben, B.N., Eck, T.F., Slutsker, I., Tanré, D., Buis, J.P., Setzer, A., Vermote, E., Reagan, J.A., Kaufman, Y.J., Nakajima, T., Lavenu, F., Jankowiak, I., Smirnov, A., 1998. AERONET—A federated instrument network and data archive for aerosol characterization. Remote Sens. Environ. 66 (1), 1–16. https://doi.org/10.1016/S0034-4257(98)00031-5.

Kaufman, Y.J., Tanré, D., Boucher, O., 2002. A satellite view of aerosols in the climate system. Nature 419, 215–223. https://doi.org/10.1038/nature01091.

Koepke, P., 1984. Effective reflectance of oceanic whitecaps. Appl. Opt. 23, 1816–1824. https://doi.org/10.1364/AO.23.001816.

King, M.D., Kaufman, Y.J., Tanré, D., Nakajima, T., 1999. Remote sensing of tropospheric aerosols from space: past, present, and future. Bull. Am. Meteorol. Soc. 80, 2229–2259. https://doi.org/10.1175/1520-0477(1999)080<2229:RSOTAF>2.0.CO;2.

Lamquin, N., Clerc, S., Bourg, L., Donlon, C., 2020. OLCI A/B tandem phase analysis, part 1: level 1 homogenisation and harmonisation. Remote Sens. 12 (11), 1804.

Lee, J., Hsu, N.C., Sayer, A.M., Bettenhausen, C., Yang, P., 2017. AERONET-based nonspherical dust optical models and effects on the VIIRS deep blue/SOAR over water aerosol product. J. Geophys. Res. Atmos. 122, 10,384–10,401. https://doi.org/10.1002/2017JD027258.

Levy, R.C., Mattoo, S., Munchak, L.A., Remer, L.A., Sayer, A.M., Patadia, F., Hsu, N.C., 2013. The collection 6 MODIS aerosol products over land and ocean. Atmos. Meas. Tech. 6 (11), 2989–3034. https://doi.org/10.5194/amt-6-2989-2013.

Li, X., Strahler, A.H., 1992. Geometric-optical bidirectional reflectance modeling of the discrete crown vegetation canopy: effect of crown shape and mutual shadowing. IEEE Trans. Geosci. Remote Sens. 30 (2), 276–292. https://doi.org/10.1109/36.134078.

Li, L., Dubovik, O., Derimian, Y., Schuster, G.L., Lapyonok, T., Litvinov, P., Ducos, F., Fuertes, D., Chen, C., Li, Z., Lopatin, A., Torres, B., Che, H., 2019. Retrieval of aerosol components directly from satellite and ground-based measurements. Atmos. Chem. Phys. 13409–13443. https://doi.org/10.5194/acp-19-13409-2019.

Li, L., Che, H., Zhang, X., Chen, C., Chen, X., Gui, K., Liang, Y., Wang, F., Derimian, Y., Fuertes, D., Dubovik, O., Zheng, Y., Zhang, L., Guo, B., Wang, Y., Zhang, X., 2022. A satellite-measured view of aerosol component content and optical property in a haze-polluted case over North China plain. Atmos. Res. 266, 105958 https://doi.org/10.1016/J.ATMOSRES.2021.105958.

Litvinov, P., Hasekamp, O., Cairns, B., 2011a. Models for surface reflection of radiance and polarized radiance: comparison with airborne multi-angle photopolarimetric measurements and implications for modeling top-of-atmosphere measurements. Remote Sens. Environ. 115 (2), 781–792. https://doi.org/10.1016/j.rse.2010.11.005.

Litvinov, P., Hasekamp, O., Cairns, B., Mishchenko, M., 2011b. Semi-empirical BRDF and BPDF models applied to the problem of aerosol retrievals over land: Testing on airborne data and implications for modeling of top-of-atmosphere measurements. In: Polarimetric Detection, Characterization and Remote Sensing. Springer, Dordrecht.

Lopatin, A., Dubovik, O., Chaikovsky, A., Goloub, P., Lapyonok, T., Tanré, D., Litvinov, P., 2013. Enhancement of aerosol characterization using synergy of lidar and sun-photometer coincident observations: the GARRLiC algorithm. Atmos. Meas. Tech. 6 (8), 2065–2088. https://doi.org/10.5194/amt-6-2065-2013.

Lopatin, A., Dubovik, O., Fuertes, D., Stenchikov, G., Lapyonok, T., Veselovskii, I., Wienhold, F.G., Shevchenko, I., Hu, Q., Parajuli, S., 2021. Synergy processing of diverse ground-based re-mote sensing and in situ data using GRASP algorithm: applications to radiometer, lidar and ra-diosonde observations. Atmos. Meas. Tech. 14 (3), 2575–2614. https://doi.org/10.5194/amt-14-2575-2021.

Mallet, M., Nabat, P., Johnson, B., Michou, M., Haywood, J.M., Chen, C., Dubovik, O., 2021. Climate models generally underrepresent the warming by Central Africa biomass-burning aerosols over the Southeast Atlantic. Sci. Adv. 7 https://doi.org/10.1126/sciadv.abg9998 eabg9998.

Mei, L., Rozanov, V., Vountas, M., Burrows, J.P., Richter, A., 2018. XBAER-derived aerosol optical thickness from OLCI/Sentinel-3 observation. Atmos. Chem. Phys. 18, 2511–2523. https://doi.org/10.5194/acp-18-2511-2018.

Mischenko, M., Travis, L., 1997. Satellite retrieval of aerosol properties over the ocean using polarization as well intensity of reflected sunlight. J. Geophys. Res. Atmos. 102 (D14), 16989–17013. https://doi.org/10.1029/96JD02425.

Monahan, E.C., O'Muircheartaigh, L., 1980. Optimal power-law description of oceanic whitecap coverage dependence on wind speed. J. Phys. Oceanogr. 10, 2094–2099. https://doi.org/10.1175/1520-0485(1980)010<2094:OPLDOO>2.0.CO;2.

Popp, T., de Leeuw, G., Bingen, C., Brühl, C., Capelle, V., Chedin, A., Clarisse, L., Dubovik, O., Grainger, R., Griesfeller, J., Heckel, A., Kinne, S., Klüser, L., Kosmale, M., Kolmonen, P., Lelli, L., Litvinov, P., Mei, L., North, P., Pinnock, S., Povey, A., Robert, C., Schulz, M., Sogacheva, L., Stebel, K., Stein Zweers, D., Thomas, G., Tilstra, L., Vandenbussche, S., Veefkind, P., Vountas, M., Xue, Y., 2016. Development, production and evaluation of aerosol climate data records from European satellite observations (Aerosol_cci). Remote Sens. 8, 421. https://doi.org/10.3390/rs8050421.

Pöschl, U., 2005. Atmospheric aerosols: composition, transformation, climate and health effects. Angew. Chem. Int. Ed. 44, 7520–7540. https://doi.org/10.1002/anie.200501122.

Puthukkudy, A., Martins, J.V., Remer, L.A., Xu, X., Dubovik, O., Litvinov, P., Mcbride, B., Burton, S., Barbosa, H.M.J., 2020. Retrieval of aerosol properties from Airborne Hyper Angular Rainbow Polarimeter (AirHARP) observations during ACEPOL 2017. Atmos. Meas. Tech. https://doi.org/10.5194/amt-13-5207-2020.

Rast, M., Bezy, J.L., Bruzzi, S., 1999. The ESA medium resolution imaging spectrometer MERIS a review of the instrument and its mission. Int. J. Remote Sens. 20 (9), 1681–1702. https://doi.org/10.1080/014311699212416.

Remer, L.A., Kaufman, Y.J., Tanré, D., Mattoo, S., Chu, D.A., Martins, J.V., Li, R.-R., Ichoku, C., Levy, R.C., Kleidman, R.G., Eck, T.F., Vermote, E., Holben, B.N., Remer, L.A., Kaufman, Y.J., Tanré, D., Mattoo, S., Chu, D.A., Martins, J.V., Li, R.-R., Ichoku, C., Levy, R.C., Kleidman, R.G., Eck, T.F., Vermote, E., Holben, B.N., 2005. The MODIS aerosol algorithm, products, and validation. J. Atmos. Sci. 62 (4), 947–973. https://doi.org/10.1175/JAS3385.1.

Remer, L.A., Levy, R.C., Mattoo, S., Tanr, D., Gupta, P., Shi, Y., Sawyer, V., Munchak, L. A., Zhou, Y., Kim, M., Ichoku, C., Patadia, F., Li, R., Gass, S., 2020. The dark target algorithm for observing the global aerosol system : past, present, and future. Remote Sens. https://doi.org/10.3390/rs12182900.

Ross, J., 1981. The Radiation Regime and Architecture of Plant Stands. Dr W. Junk Publishers, The Hague, Netherlands.

Samset, B.H., Stjern, C.W., Andrews, E., Kahn, R.A., Myhre, G., Schulz, M., Schuster, G.L., 2018. Aerosol absorption: progress towards global and regional constraints. Curr. Clim. Chang. Rep. 4 (2), 65–83. https://doi.org/10.1007/s40641-018-0091-4.

Sayer, A.M., Hsu, N.C., Bettenhausen, C., Ahmad, Z., Holben, B.N., Smirnov, A., Thomas, G.E., Zhang, J., 2012. SeaWiFS ocean aerosol retrieval (SOAR): algorithm, validation, and comparison with other data sets. J. Geophys. Res. Atmos. 117 (D03206), 1–17. https://doi.org/10.1029/2011JD016599.

Sayer, A.M., Munchak, L.A., Hsu, N.C., Levy, R.C., Bettenhausen, C., Jeong, M.-J., 2014. MODIS collection 6 aerosol products: comparison between Aqua's e-deep blue, dark target, and "merged" data sets, and usage recommendations. J. Geophys. Res. Atmos. 119 (24), 13,965–13,989. https://doi.org/10.1002/2014JD022453.

Sayer, A.M., Hsu, N.C., Lee, J., Kim, W.V., Dubovik, O., Dutcher, S.T., Huang, D., Litvinov, P., Lyapustin, A., Tackett, J.L., Winker, D.M., 2018. Validation of SOAR VIIRS over-water aerosol retrievals and context within the global satellite aerosol data record. J. Geophys. Res. Atmos. 123 https://doi.org/10.1029/2018JD029465, 2018JD029465.

Schaaf, C., Wang, Z., 2015. MCD43C3 MODIS/Terra+Aqua BRDF/Albedo Albedo Daily L3 Global 0.05Deg CMG V006 [Data set]. NASA EOSDIS Land Processes DAAC. https://doi.org/10.5067/MODIS/MCD43C3.006. Accessed 2020-09-14 from.

Schuster, G.L., Espinosa, W.R., Ziemba, L.D., Beyersdorf, A.J., Rocha-Lima, A., Anderson, B.E., Martins, J.V., Dubovik, O., Ducos, F., Fuertes, D., Lapyonok, T., Shook, M., Derimian, Y., Moore, R.H., 2019. A laboratory experiment for the statistical evaluation of aerosol retrieval (STEAR) algorithms. Remote Sens. 11 (5), 498. https://doi.org/10.3390/rs11050498.

Schutgens, N., Dubovik, O., Hasekamp, O., Torres, O., Jethva, H., Leonard, P.J.T., Litvinov, P., Redemann, J., Shinozuka, Y., de Leeuw, G., Kinne, S., Popp, T., Schulz, M., Stier, P., 2021. AEROCOM/AEROSAT AAOT & SSA study, part I: evaluation and intercomparison of satellite measurements. Atmos. Chem. Phys. 21 (9), 6895–6917. https://doi.org/10.5194/acp-21-6895-2021.

Sentinel-3 OLCI User Guides, 2022. https://sentinel.esa.int/web/sentinel/user-guides/sentinel-3-olci.

Sinyuk, A., Holben, B., Eck, T., Giles, D., Slutsker, I., Korkin, S., Schafer, J., Smirnov, A., Sorokin, M., Lyapustin, A., 2020. The AERONET version 3 aerosol retrieval algorithm, associated uncertainties and comparisons to version 2. Atmos. Meas. Tech. 13, 3375–3411. https://doi.org/10.5194/amt-13-3375-2020.

Smirnov, A., Holben, B.N., Eck, T.F., Dubovik, O., Slutsker, I., 2000. Cloud-screening and quality control algorithms for the AERONET database. Remote Sens. Environ. 73 (3), 337–349. https://doi.org/10.1016/S0034-4257(00)00109-7.

Smirnov, A., Holben, B.N., Slutsker, I., Giles, D.M., McClain, C.R., Eck, T.F., Sakerin, S. M., Macke, A., Croot, P., Zibordi, G., Quinn, P.K., Sciare, J., Kinne, S., Harvcy, M., Smyth, T.J., Piketh, S., Zielinski, T., Proshutinsky, A., Goes, J.I., Nelson, N.B., Larouche, P., Radionov, V.F., Goloub, P., Krishna Moorthy, K., Matarrese, R., Robertson, E.J., Jourdin, F., 2009. Maritime aerosol network as a component of aerosol robotic network. J. Geophys. Res. Atmos. 114, 1–10. https://doi.org/10.1029/2008JD011257.

Smirnov, A., Holben, B.N., Giles, D.M., Slutsker, I., O Neill, N.T., Eck, T.F., Macke, A., Croot, P., 2011. Maritime aerosol network as a component of AERONET – first results and comparison with global aerosol models and satellite retrievals. Atmos. Meas. Tech. 4 (3), 583–597. https://doi.org/10.5194/amt-4-583-2011.

SNAP, 2022. (Sentinel Application Platform) Version 6.0. https://step.esa.int/main/toolboxes/snap/.

Torres, B., Fuertes, D., 2021. Characterization of aerosol size properties from measurements of spectral optical depth: a global validation of the GRASP-AOD code using long-term AERONET data. Atmos. Meas. Tech. 14, 4471–4506. https://doi.org/10.5194/amt-14-4471-2021.

Stier, P., Seinfeld, J.H., Kinne, S., Boucher, O., 2007. Aerosol absorption and radiative forcing. Atmos. Chem. Phys. 7, 5237–5261. https://doi.org/10.5194/acp-7-5237-2007.

Torres, B., Dubovik, O., Fuertes, D., Schuster, G., Cachorro, V.E., Lapyonok, T., Goloub, P., Blarel, L., Barreto, A., Mallet, M., Toledano, C., Tanré, D., 2017. Advanced characterisation of aerosol size properties from measurements of spectral optical depth using the GRASP algorithm. Atmos. Meas. Tech. 10 (10), 3743–3781. https://doi.org/10.5194/amt-10-3743-2017.

Zhang, X., Li, L., Chen, C., Zheng, Y., Dubovik, O., Derimian, Y., Lopatin, A., Gui, K., Wang, Y., Zhao, H., Liang, Y., Holben, B., Che, H., Zhang, X., 2021. Extensive characterization of aerosol optical properties and chemical component concentrations: application of the GRASP/component approach to long-term AERONET measurements. Sci. Total Environ. 812, 152553 https://doi.org/10.1016/j.scitotenv.2021.152553.

Zhou, Y., Levy, R.C., Remer, L.A., Mattoo, S., Espinosa, W.R., 2020. Dust aerosol retrieval over the oceans with the MODIS/VIIRS dark target algorithm: 2. Nonspherical dust model. Earth Space Sci. 7 https://doi.org/10.1029/2020EA00122 e2020EA001222.